

ANNUAL REPORT LETTER

TASK DESCRIPTION FOR VENTILATION MODELING FOR APRIL 1, 2006 TO MARCH 31, 2007

Project Title: Nye County Ventilation Modeling
Author and PI: George Danko, Ph.D.
Report Period: April 1, 2006-March 31, 2007
Date of Report: July 30, 2007

Summary

During the FY06 the following 4 tasks were performed and reported. The results have been published and presented¹⁻⁷. The results were also reported continuously in the form of monthly progress reports. This work is a continuation of modeling tasks conducted in the previous grant year (April 1, 2005 to March 31, 2006).

1. Task 1: Examine the Potential Significance of Water Vapor Migration Between the Network of Drifts for the Baseline Repository Design (FY05 - FY06)

1.1 Model update

Model update included the following main changes:

- Detailed in-drift model configuration with under and above drip shield regions.
- Unheated 80-m drift sections at both ends.
- 600-m heated section versus 714-m heated drift in the 2005, FY 04 study report.
- Recent addition of air flow CFD solver.
- Inclusion of latent heat of condensation at the unheated drift sections.

1.2 One-directional air flow studies

A small, post-closure, buoyancy-driven air infiltration through the drift bulkhead to neighboring drifts was assumed. The air flow variation with time is shown in Figure 1, selected based on a previous, natural ventilation model⁸. The temperature and relative humidity variations at year 500 are shown in Figure 2 for two different air flow directions (from left to right, and from right to left) in the emplacement drift.

The effect of one-directional flow is estimated to be about 15°C in temperature in the cold section and no significant change in the heated section. An overall effect of about 10% RH reduction is also seen from the model results. The explanation of this phenomenon is that the cold, condensing drift section dries out some of the moisture content of the air, increasing its capacity to absorb humidity during the flow across the drift, irrespective of the flow direction.

1.3 Recirculation air flow studies

New model calculations were performed using a new natural air flow model element in the Computational Fluid Dynamics (CFD) model of one emplacement drift. The MULTIFLUX

code modification and verification was supported by the SNT Project ⁹. The modeling work of a more complex configuration was performed for NYE county reported in this report. The same model configuration, except with the line averaged heat load was used for MF testing. The new element of the model configuration was that the heat and mass transport within the drift air space included the effects of carrying air velocities. The velocity field was autonomously calculated in MULTIFLUX, solving for natural airflow, driven by temperature and humidity differences, resulting in natural buoyancy effects. The simulation provided a fully balanced solution between the heat and mass transport processes in the drift air space and in the surrounding rock mass.

In order to depict the three-dimensional velocity field from the numerical solution in simple, two-dimensional figures, lumped air nodes are used as follows. The air1, air2, air3, and air4 designate air nodes inside the drip shield air space at a given cross section along the drift, shown in Figure 3. The air5, air 6, air7, and air8 identify air nodes outside the drip shield in the air space at a given cross section along the drift, shown in Figure 4. Note that the average of all four air velocities weighted with their corresponding flow cross sections either above or below the drip shield would give approximately zero average since the net average axial air mass flow rate is zero. It is only the circulation which is non-zero in a closed air space. All four vertical air flow velocity components are averaged into one circulation velocity either above, or below the drip shield. Positive velocity in the horizontal direction means airflow from drift entrance toward the exit, from left to right. Positive velocity in the vertical direction loop means counter-clockwise circulation, shown in Figure 5. The two-dimensional, simplified representation of the large-scale airflows in the horizontal circulation direction are shown in Figures 6 through 12 for the airspace inside and outside the drip shield at seven different time instants from year 51 to year 5000. The vertical air velocities in each drift cross section and with the variation along the drift length are shown in Figures 13 through 19 for the air space inside and outside the drip shield, respectively at seven different time instants. Both horizontal and vertical re-circulation velocities show a decrease in magnitude by about a factor of three with increasing time from year 51 to year 5000.

The results show that well-defined, large-scale axial airflow re-circulation loops form in the drift. It can be seen in Figures 6 to 12 that in each half-drift section, air velocity at one or two air lines move toward the drift center and others move away toward the drift ends. The air circulation is maintained by the natural buoyancy pressure difference even in the case of a perfectly horizontal drift. The height difference within the 5.5 diameter drift and the axial temperature difference between the cold ends and the hot middle section along the drift length provide apparently enough driving force for natural re-circulation. Two main axial loops form, one above, and one below the drip shield. In either air space, the average air velocity is around 0.05 m/s over half of the drift cross section in either direction at year 1000. This gives a travel time of about two hours for convective exchange between the center and the ends of the drift at year 1000 during post closure. Note that the axial velocity at the drift center is zero, due to symmetry between the left and right side of the drift. Air circulation in the vertical plane is somewhat weaker than the recirculation in the horizontal direction. This is explained by the smaller temperature difference between hot and cold surfaces in the radial than in the horizontal direction within the emplacement drift. Apparently, it is not the temperature gradient, but rather the total, integrated temperature difference over the

circulation loop length that matters in the buoyancy driving potential. The vertical and the horizontal re-circulation air loops are inter-connected in the above drip shield and the below drip shield air spaces but the two air spaces are separated except for their connection at the drift ends. The intercommunications allow slight variations in the magnitude of the axial velocities. The new model results represent a significant success in modeling turbulent flow with a lumped-parameter CFD model, and coupling it with the rock model for mountain scale temperature distribution calculation with the MULTIFLUX software.

For comparison and model validation purposes, the equivalent, effective dispersion coefficient along the drift length was inverse-calculated from the convective moisture transport due to the velocity field. Figure 20 shows the equivalent dispersion coefficient for three different post-closure time periods. As shown, the equivalent dispersion coefficient varies with both time, and location. The range in peak values (approximately 0.07 to 0.13 m^2/s) for all time periods agrees well with the maximum value of 0.1 m^2/s from the Yucca Mountain literature for the air space outside the drip shield. The equivalent dispersion coefficient range for the air space inside the drip shield is approximately 0.05 to 0.08 m^2/s , a factor of 10 higher than the 0.006 m^2/s value published for a comparable arrangement for an emplacement drift. The good agreement for the equivalent dispersion coefficient in the above-drip shield domain is taken as a successful comparison for model calibration against published data. The poor agreement in the below-drip shield domain is worrisome, and warrants further investigation. The working hypothesis is that the calculated dispersion coefficient in the below drip shield domain in the literature did not capture the axial transport processes accurately.

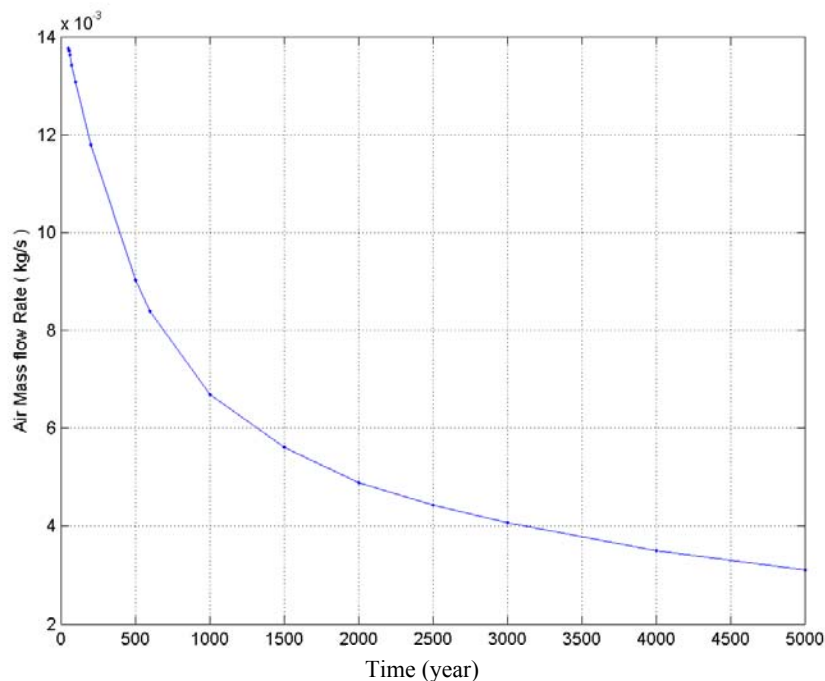


Figure 1. Air flow variation with time, used in the one-dimensional air flow studies.

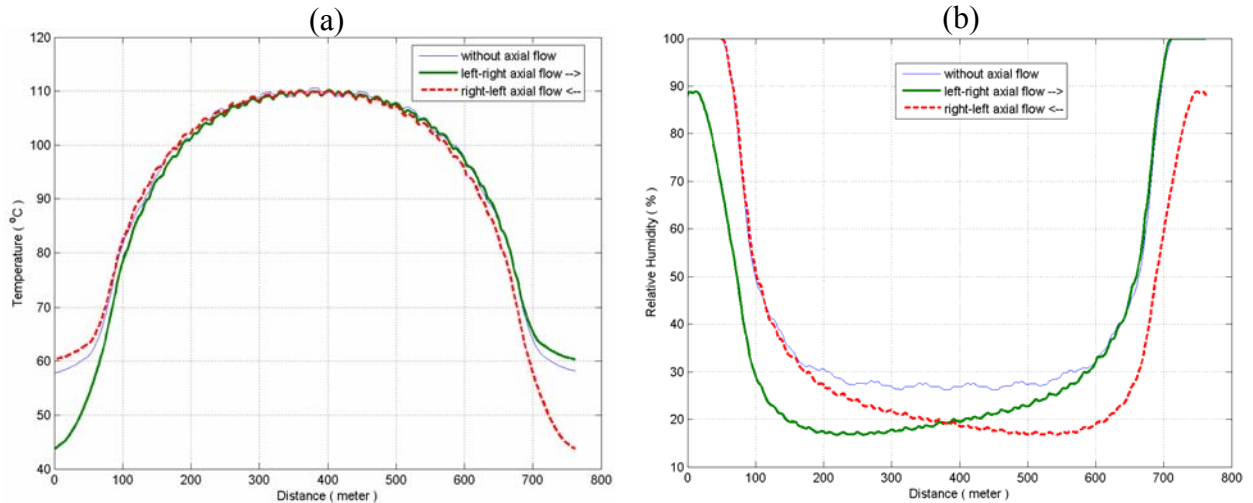


Figure 2. Temperature and relative humidity variations at year 500 under two different air flow directions in the emplacement drift.

Temperature, relative humidity, and rate of condensation distributions along the drift length are shown for selected post-closure time periods in Figures 21, 22 and 23 at three different segments of the drift wall: the roof; the sidewalls; and the floor over the invert. Significant differences are seen in the relative humidity and condensation rates over the segments of the drift circumference, while the temperature remain nearly constant. It is interesting to notice that the relative humidity and condensation rate are both higher on the floor than over the rest of the drift wall. This fact may be significant for two reasons. Firstly, the floor segment is under the drip shield and it constitutes the area which is in direct contact with the waste packages. The appearance of liquid water from condensation on the floor (and already under the drip shields) may provide aqueous transport of particles from this area towards the water table, in spite of having drip shield over the waste packages. Secondly, the floor segment and the drip shields form a relatively separated micro-tunnel from the rest of the drift air space, and the air in this micro-tunnel constitutes the primary storage environment for the waste packages. While this micro-tunnel is shielded from direct drippage from the floor, vapor is supplied at an elevated rate from the floor relative to the sidewalls and the roof, giving ample moisture source. On the other hand, the transport cross-section of the micro-tunnel is only a fraction of that of the main air space in the drift, impeding the axial transport of heat and moisture. For these reasons, modeling of the storage environment in the micro-tunnel appears to be an important task, especially considering that no project data are available for this region since other baseline models for YM^{10,11} treat the volume of the micro-tunnel as solid material with average properties, attached to the waste packages.

Figures 24 a and b compares the new, convective model results based on an explicit, three-dimensional, natural air flow field in the drift (both under, and over the drip shields) with the results from a previous, simplified model, using the equivalent dispersion coefficient. The results for temperature, relative humidity, and rate of condensation distributions along the drift length are shown in Figure 24 only for two post-closure time periods: year 1000 (a); and year 5000 (b).

Both figures depict the new, convective model results with two unheated drift sections (according to a new conceptual design arrangement) and the previous model results obtained using a constant equivalent dispersion coefficient of $0.1 \text{ m}^2/\text{s}$ and no unheated drift sections in the Task 4 model configuration (FY 04). Quite different temperature, relative humidity and rate of condensation distributions are obtained from the new model when compared to the previous model results, using different conceptual design arrangements. The two cases are shown together (the new model and the Task 4 model) to demonstrate the differences in storage environments that may be predicted depending on waste arrangement as well as model configuration.

Finally, the results of a brief sensitivity study are shown in Figures 25 and 26. The equivalent dispersion coefficient, as an easy-to-understand parameter and comparable to published data, are divided for the air space outside and inside the drip shield in Figure 25 a and b, respectively, as a function of the air flow friction loss parameter. This figure shows that the equivalent dispersion coefficient is not very sensitive to the air flow friction loss parameter. Similar results are obtained showing the effect of large-eddy, turbulent kinetic shock loss factor on the equivalent dispersion coefficient in Figures 26 a and b for inside and outside the drip shield airspaces, respectively.

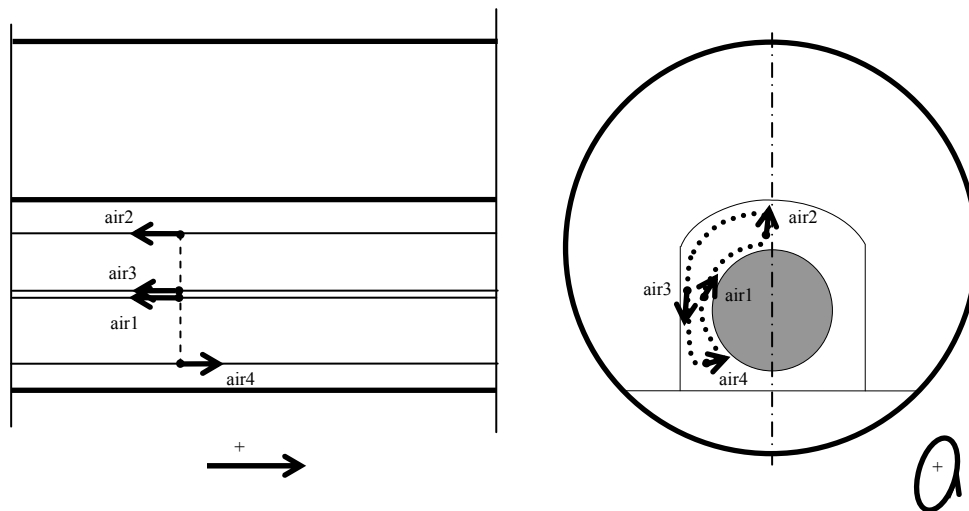


Figure 3. Definition of horizontal and vertical velocity components at a given cross section under the drip shield.

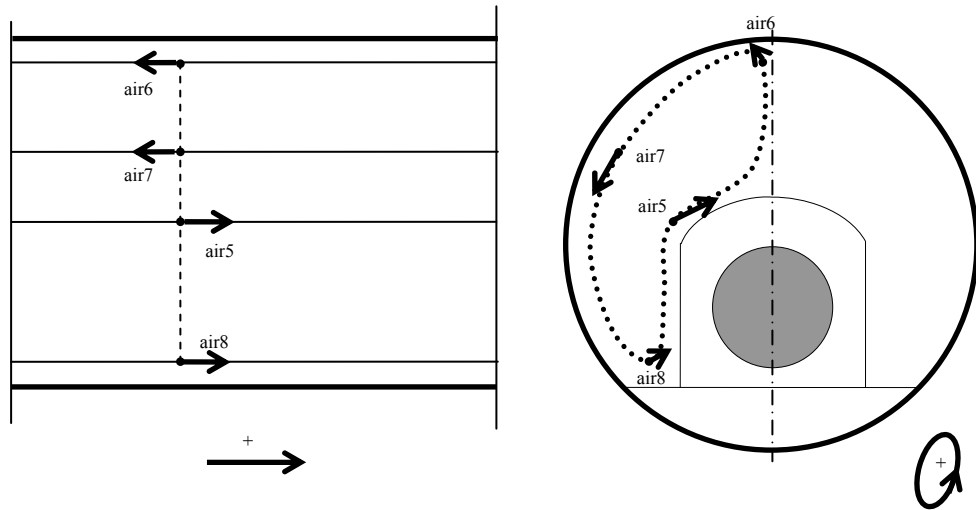


Figure 4. Definition of horizontal and vertical velocity components at a given cross section outside the drip shield.

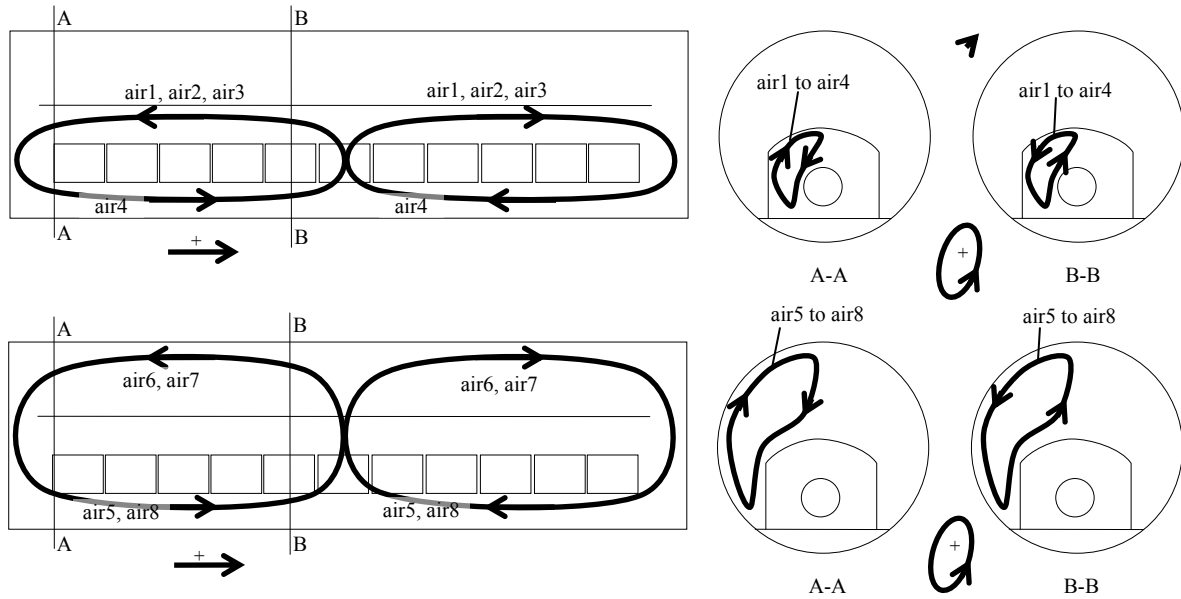


Figure 5. Drift-scale natural air flow patterns in one emplacement drift.

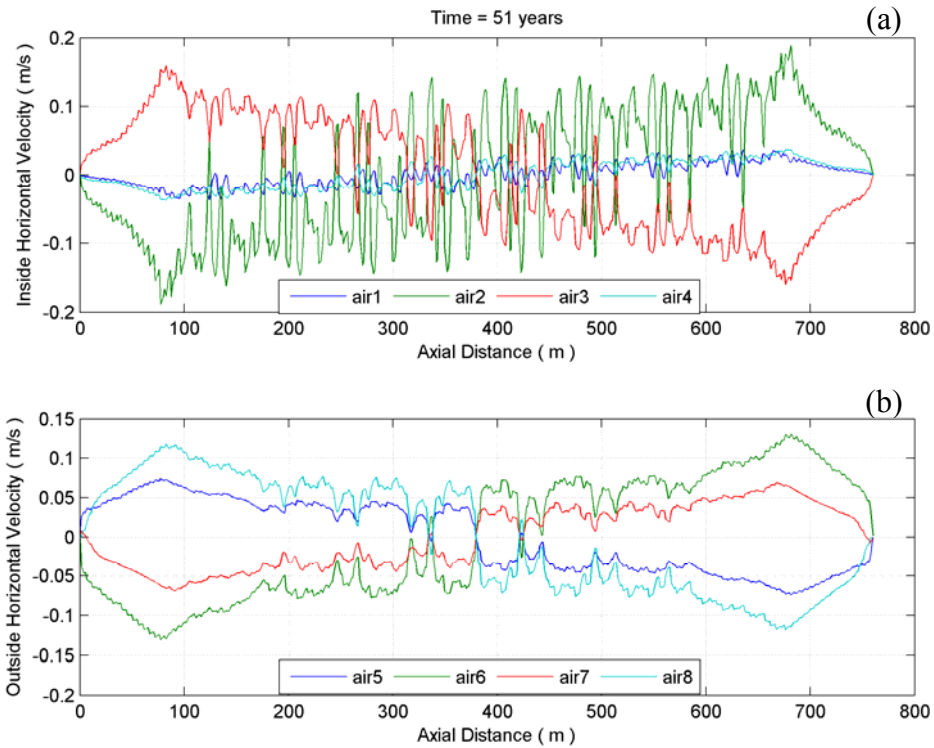


Figure 6. Horizontal air flow velocity variation along the emplacement drift (a) inside and (b) outside the drip shield at year 51.

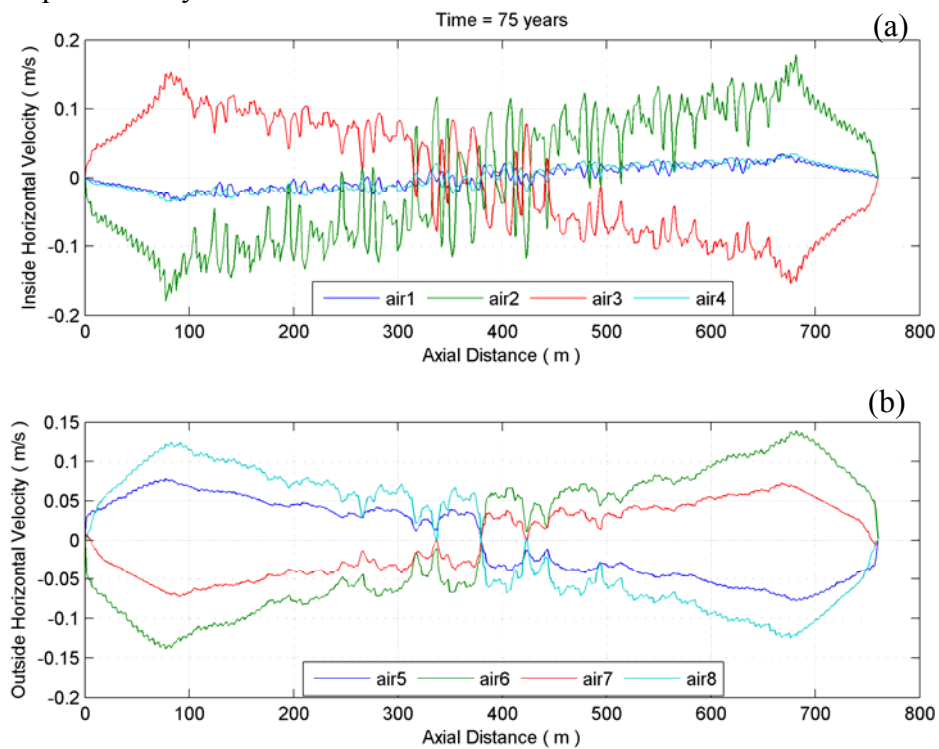


Figure 7. Horizontal air flow velocity variation along the emplacement drift (a) inside and (b) outside the drip shield at year 75.

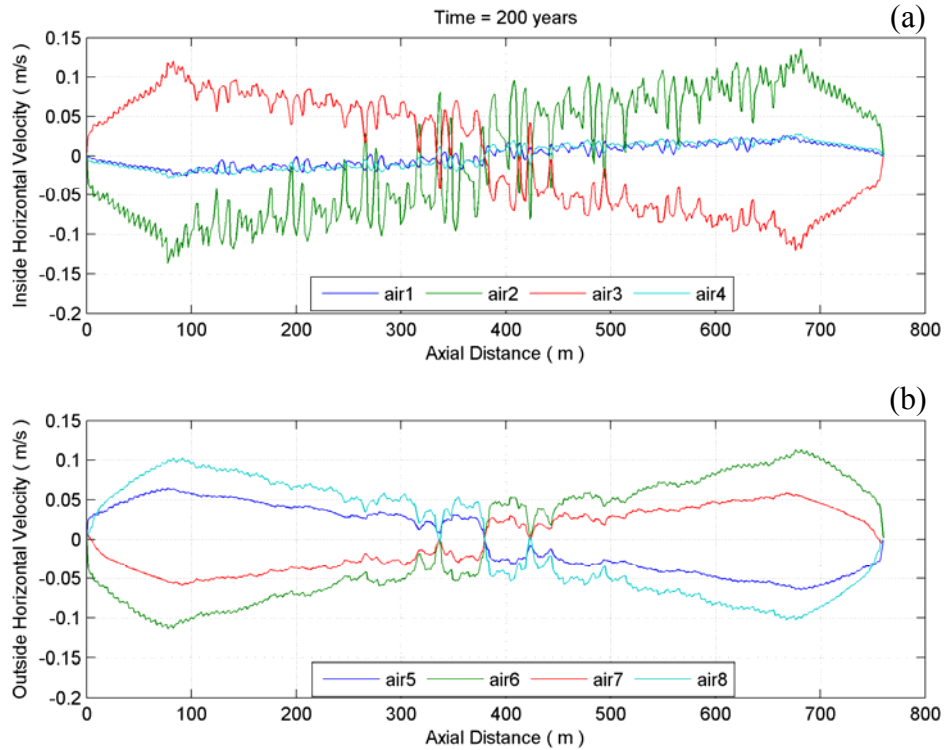


Figure 8. Horizontal air flow velocity variation along the emplacement drift (a) inside and (b) outside the drip shield at year 200.

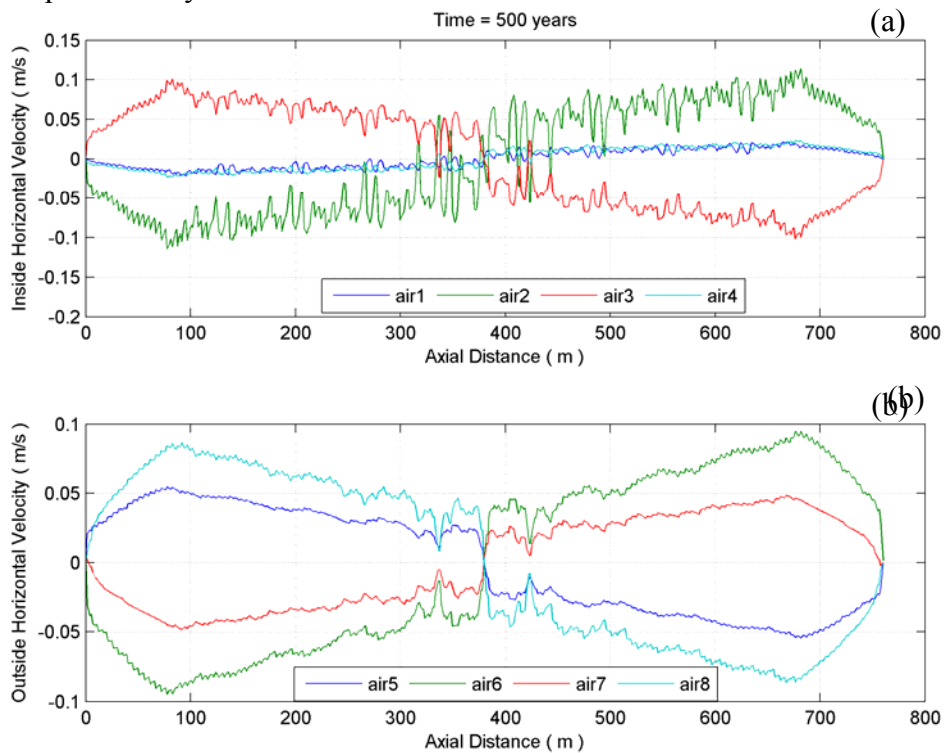


Figure 9. Horizontal air flow velocity variation along the emplacement drift (a) inside and (b) outside the drip shield at year 500.

(a)

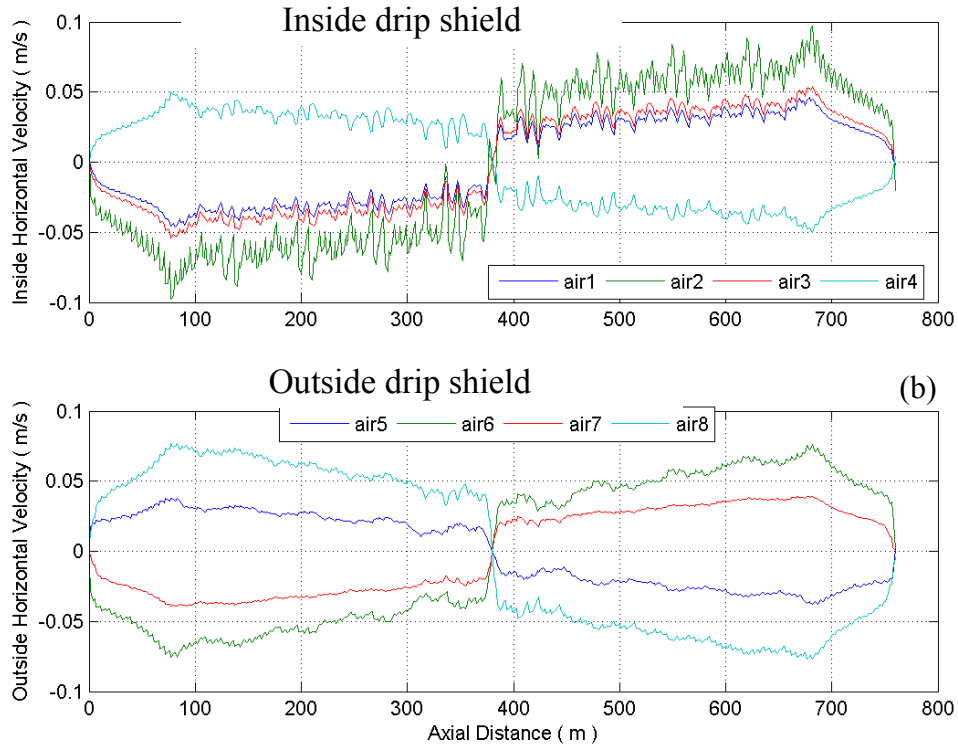


Figure 10. Air flow velocity variation in the horizontal circulation direction along the emplacement drift (a) inside and (b) outside the drip shield at year 1000.

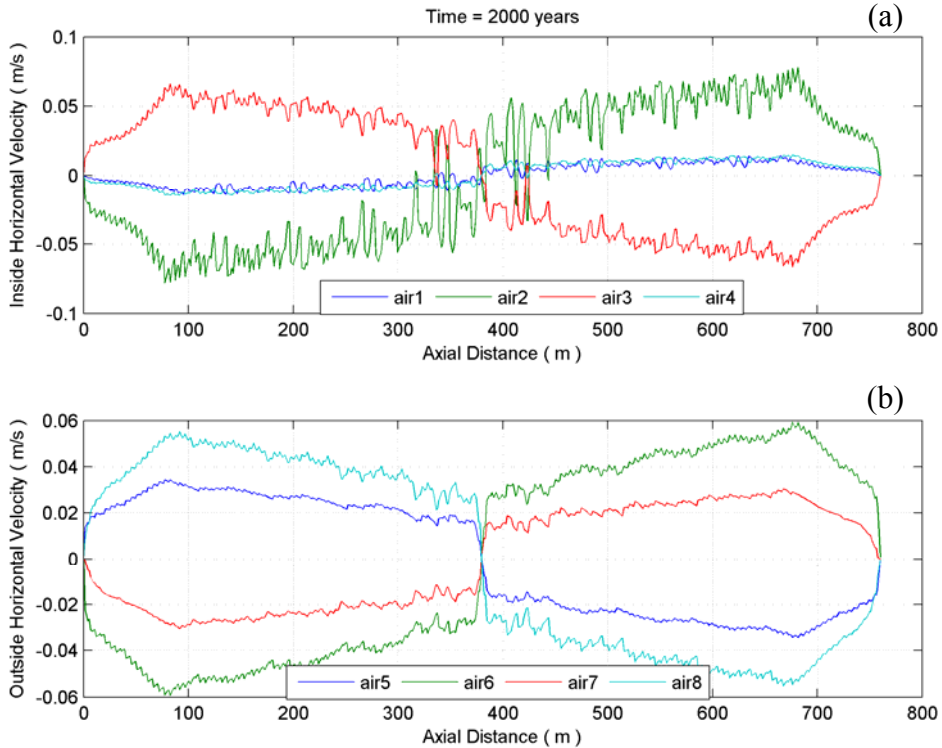


Figure 11. Horizontal air flow velocity variation along the emplacement drift (a) inside and (b) outside the drip shield at year 2000.

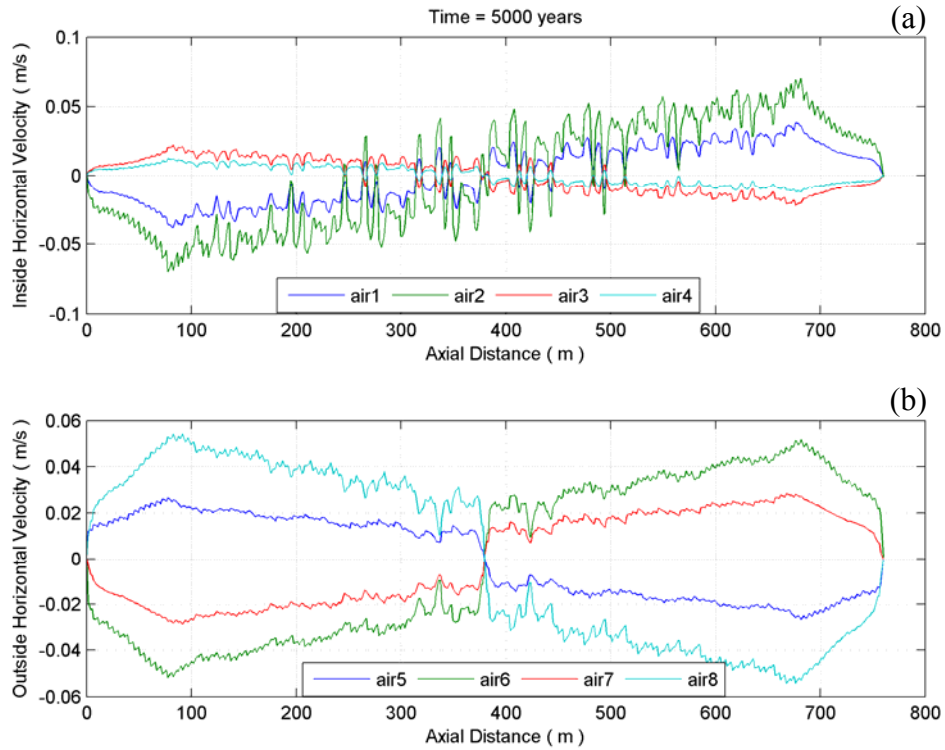


Figure 12. Horizontal air flow velocity variation along the emplacement drift (a) inside and (b) outside the drip shield at year 5000.

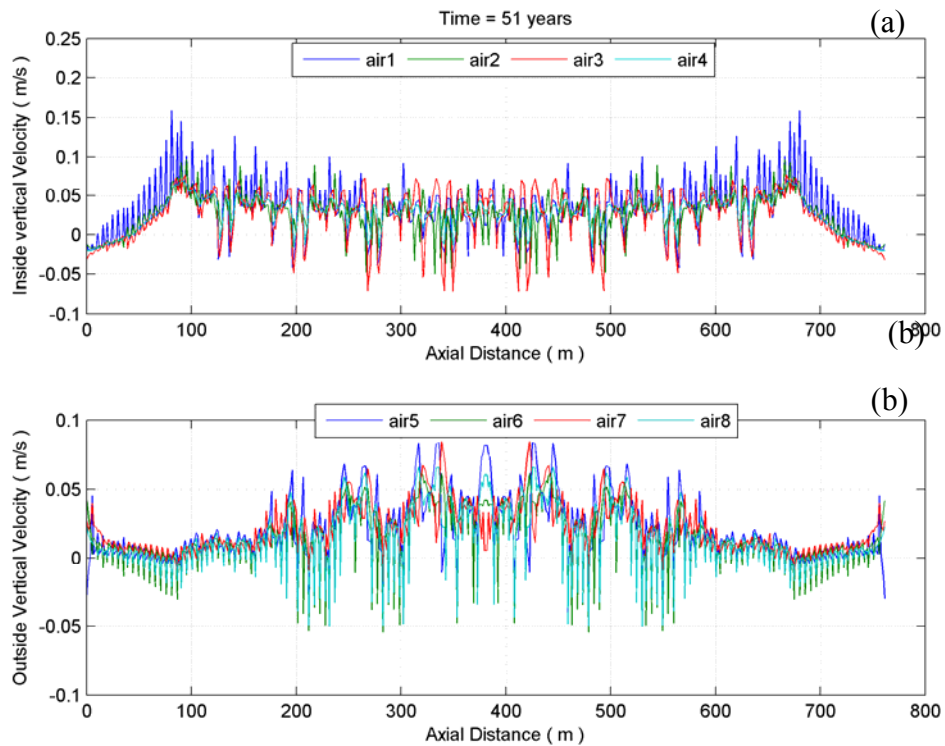


Figure 13. Vertical in-drift velocities along the drift length (a)inside and (b)outside the drip shield at year 51

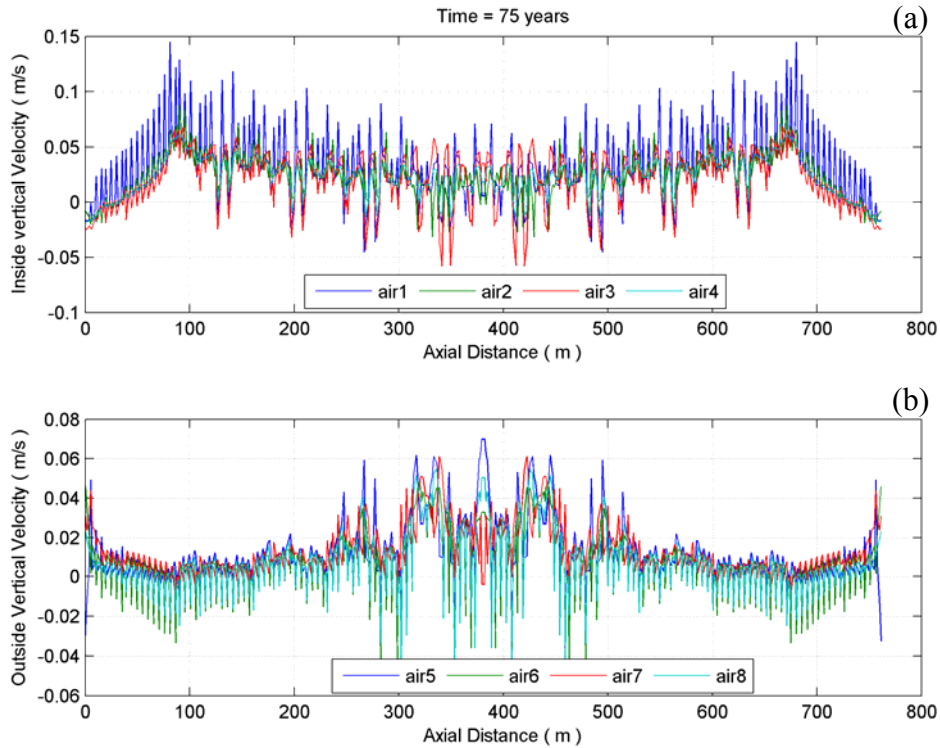


Figure 14. Vertical in-drift velocities along the drift length (a)inside and (b)outside the drip shield at year 75

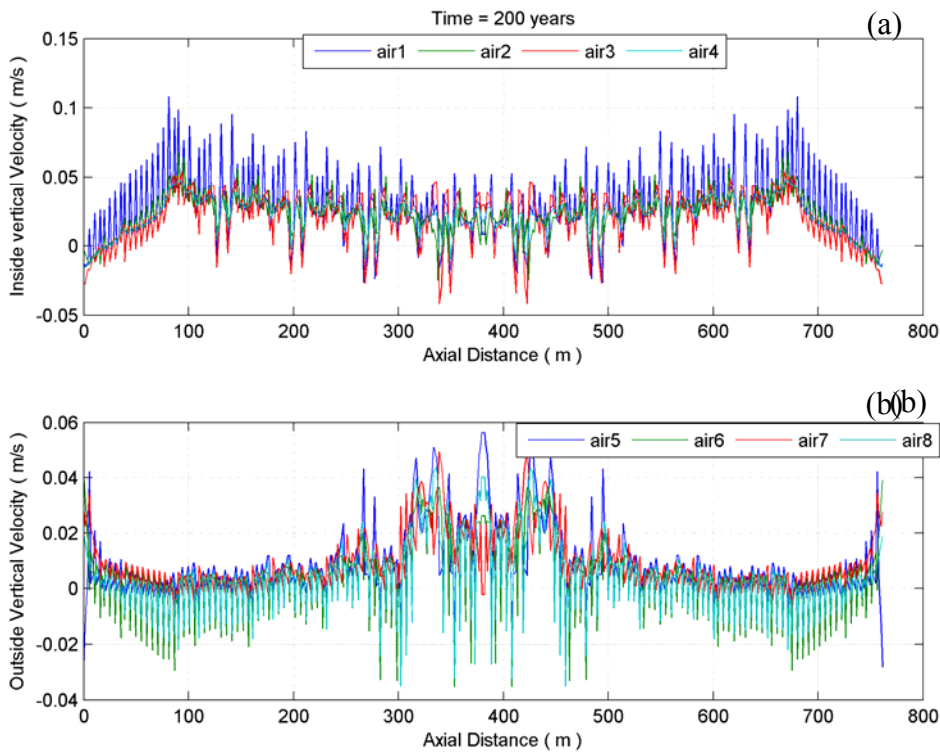


Figure 15. Vertical in-drift velocities along the drift length (a)inside and (b)outside the drip shield at year 200

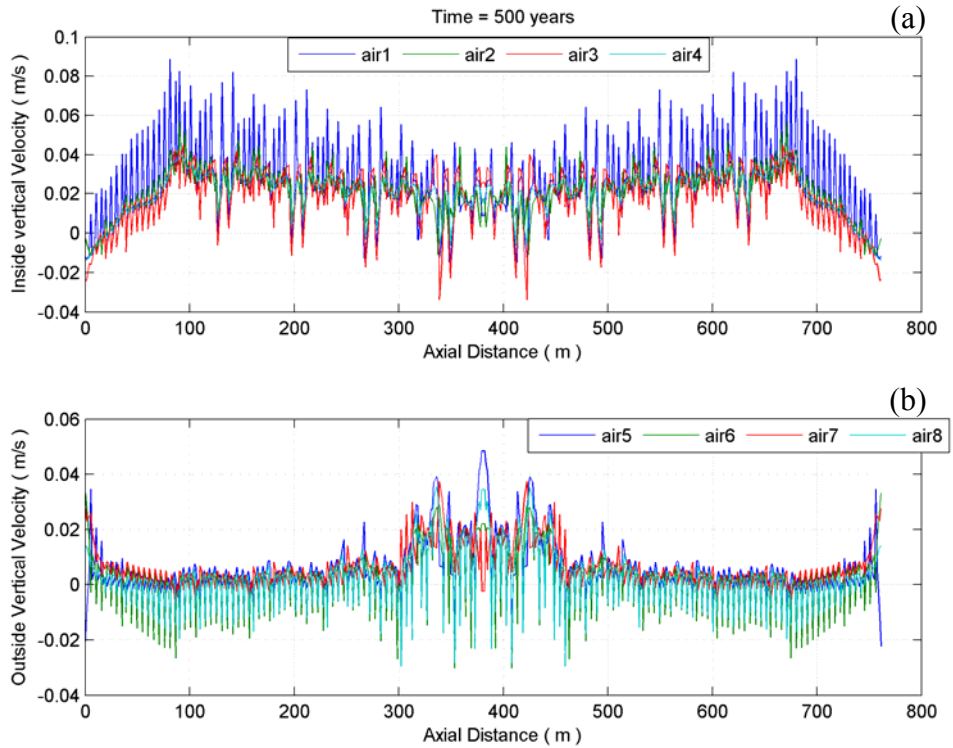


Figure 16. Vertical in-drift velocities along the drift length (a)inside and (b)outside the drip shield at year 500

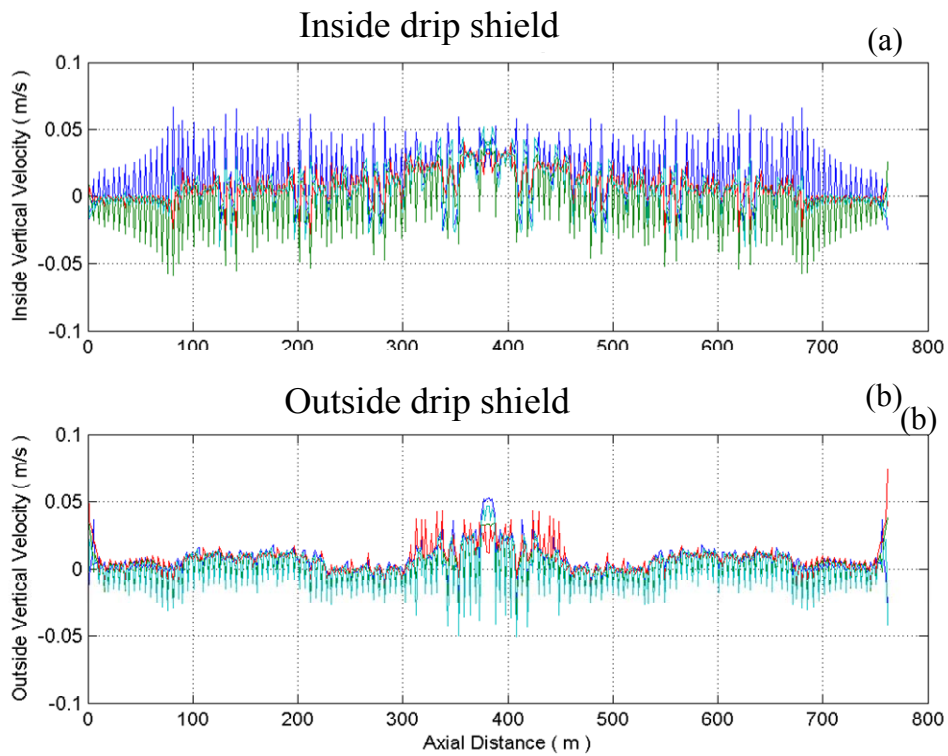


Figure 17. Vertical in-drift velocities along the drift length (a)inside and (b)outside the drip shield at year 1000

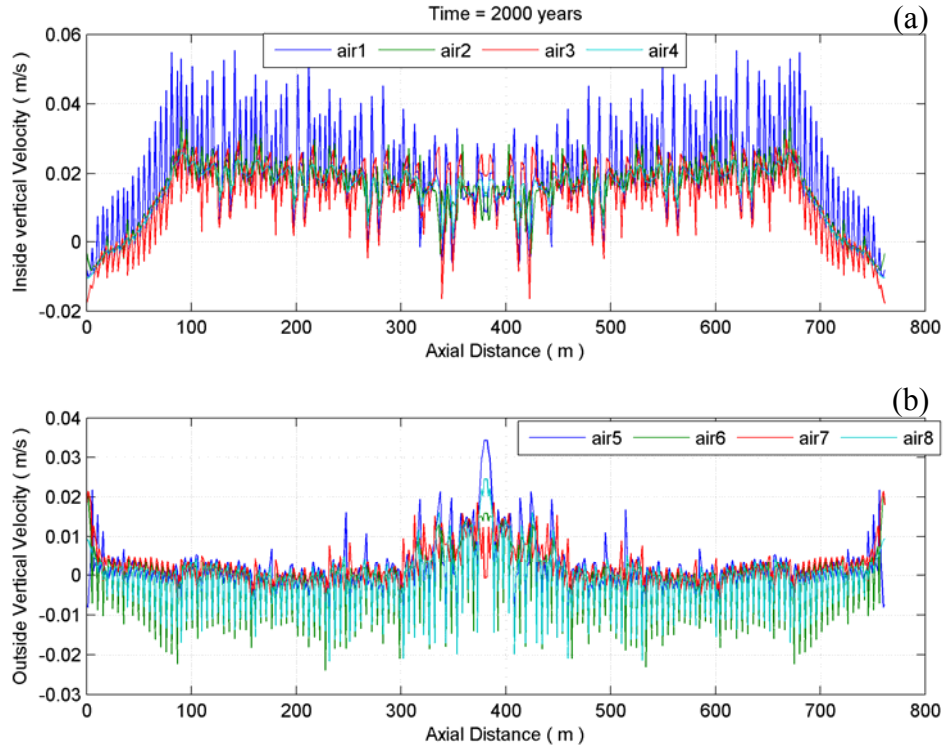


Figure 18. Vertical in-drift velocities along the drift length (a)inside and (b)outside the drip shield at year 2000

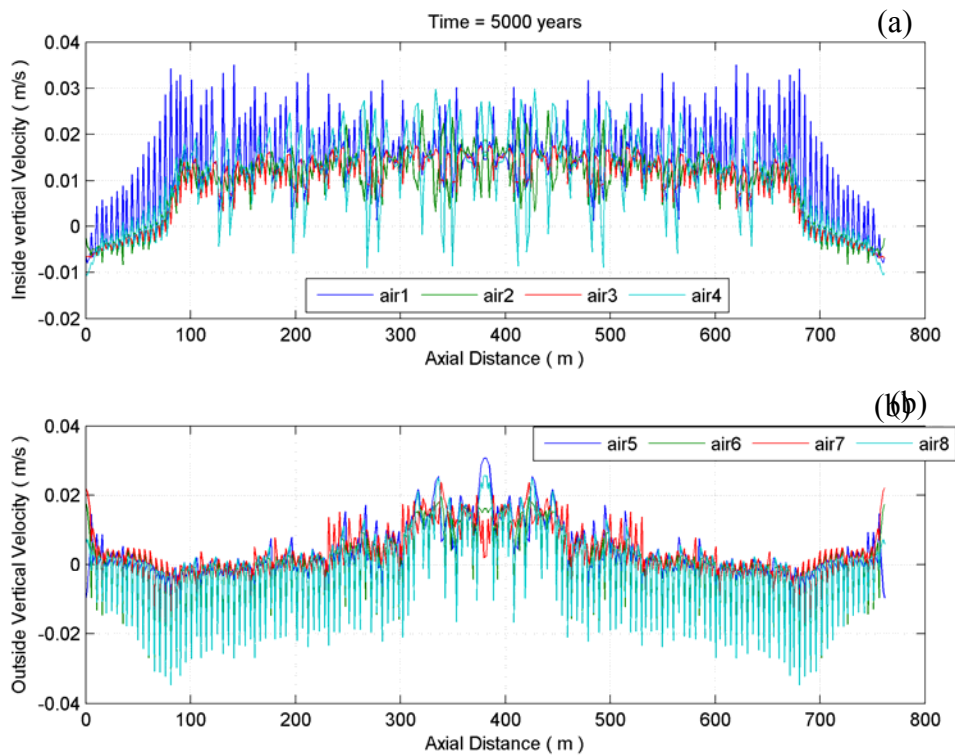


Figure 19. Vertical in-drift velocities along the drift length (a)inside and (b)outside the drip shield at year 5000

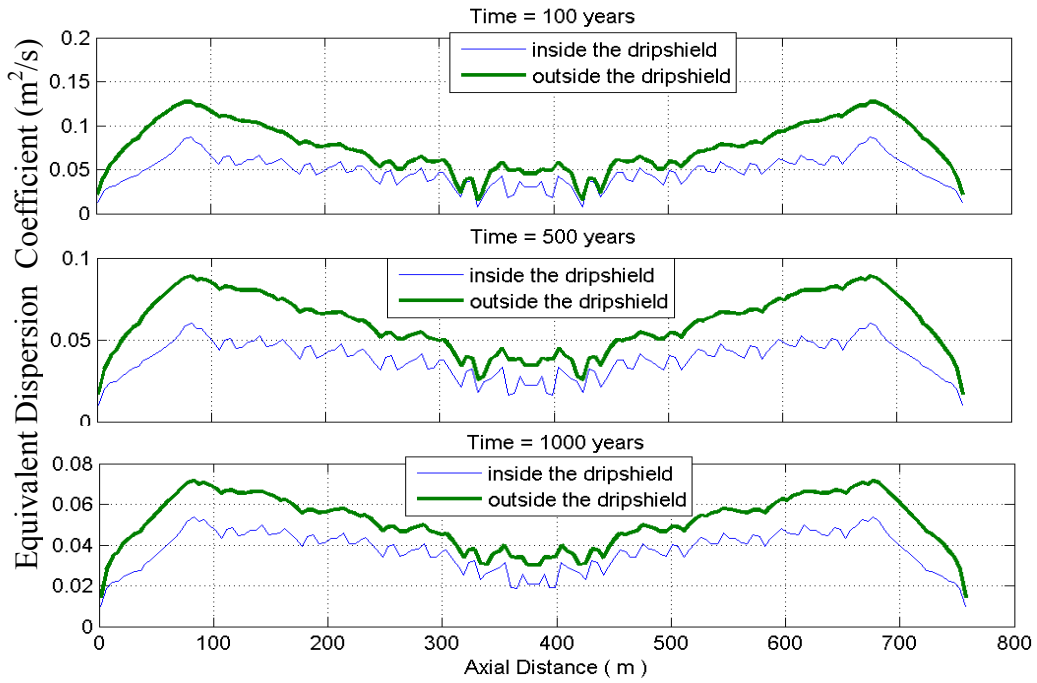


Figure 20. Equivalent dispersion coefficient at three time periods.

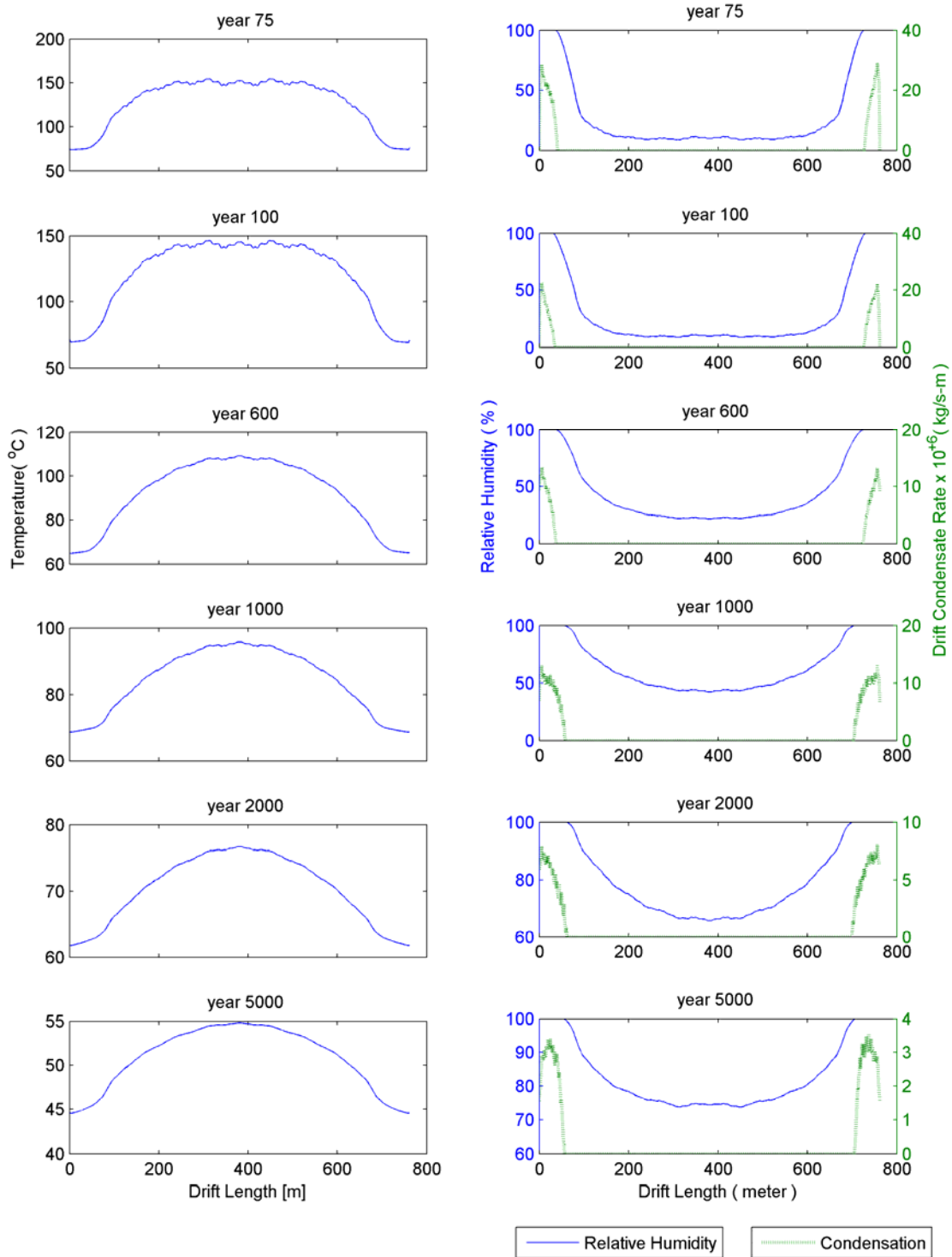


Figure 21. Temperature, relative humidity, and rate of condensation distributions along the drift length for selected post-closure time periods at the roof segment of the drift wall.

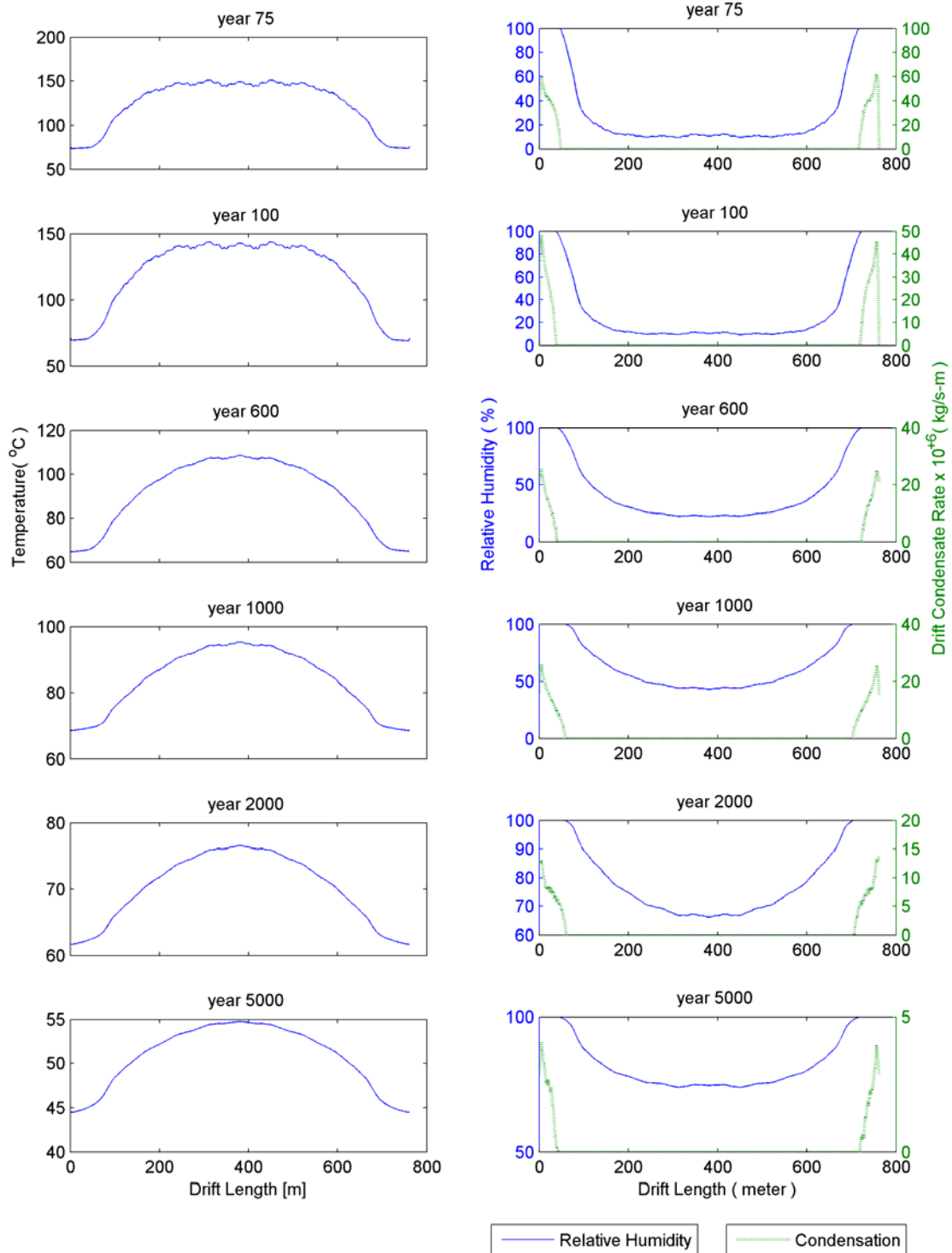


Figure 22. Temperature, relative humidity, and rate of condensation distributions along the drift length for selected post-closure time periods at the sidewall segment of the drift wall.

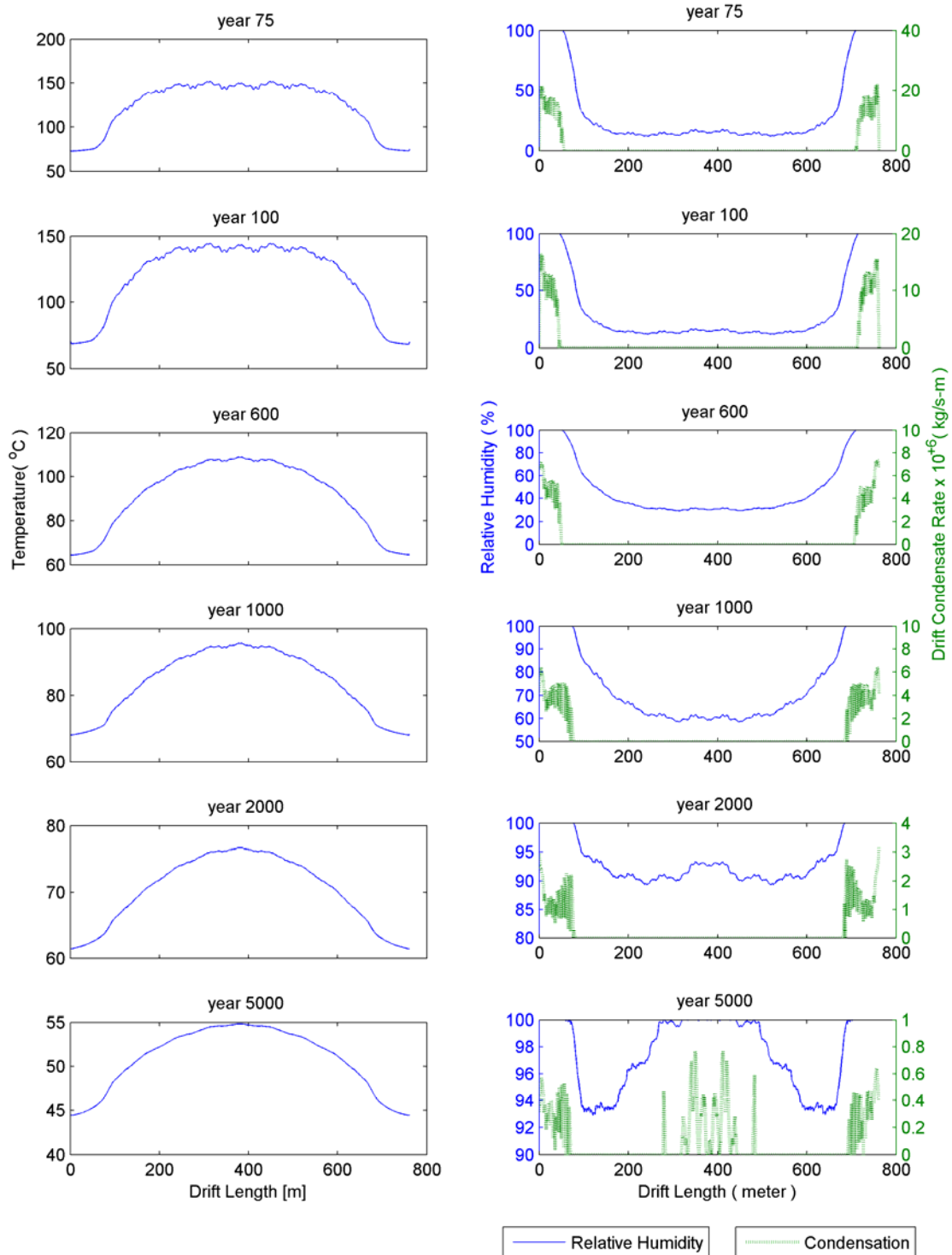


Figure 23. Temperature, relative humidity, and rate of condensation distributions along the drift length for selected post-closure time periods at the floor segment of the drift wall over the invert.

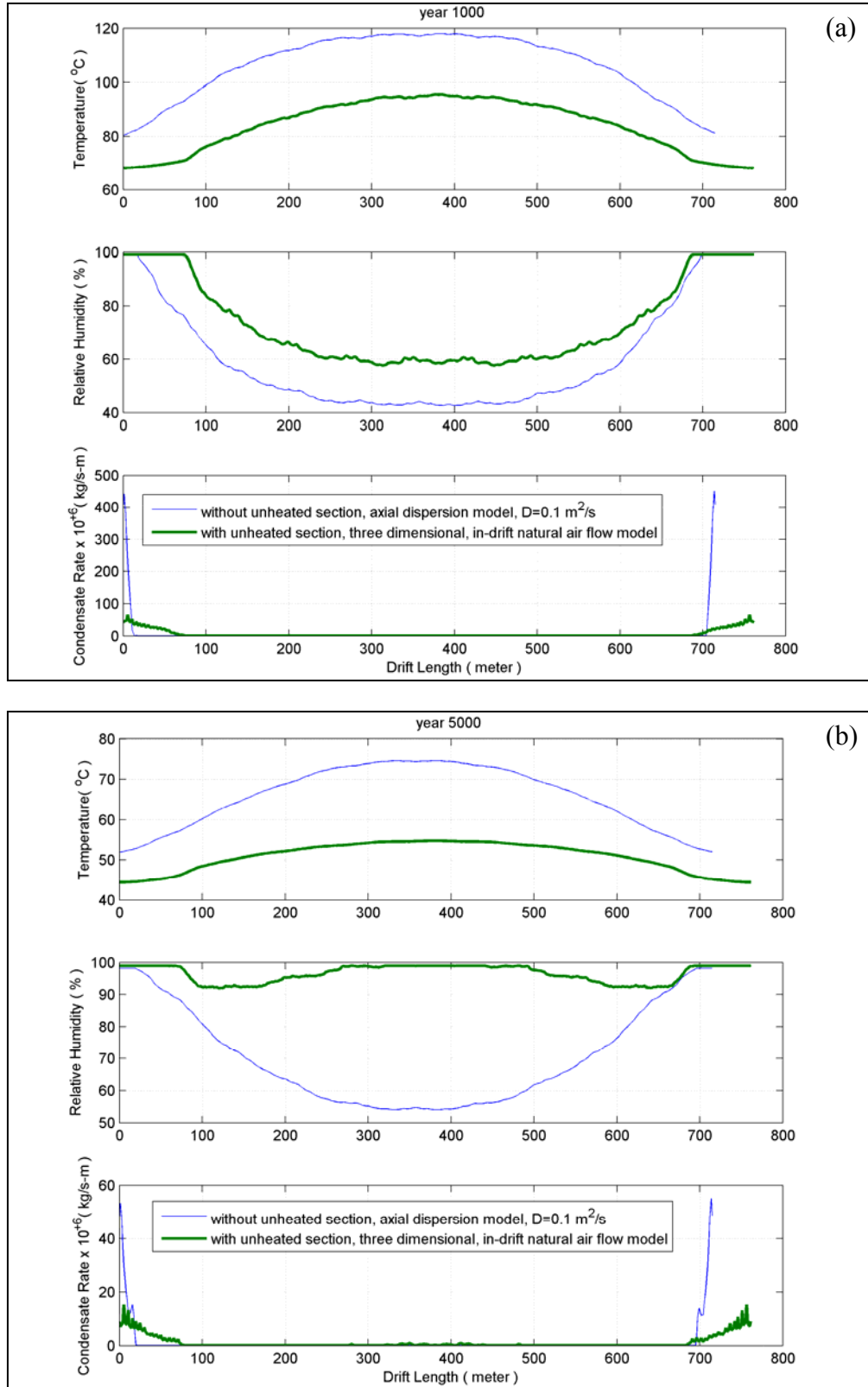


Figure 24. Temperature, relative humidity, and rate of condensation distributions along the drift length for two post-closure time periods: year 1000 (a); and year 5000 (b).

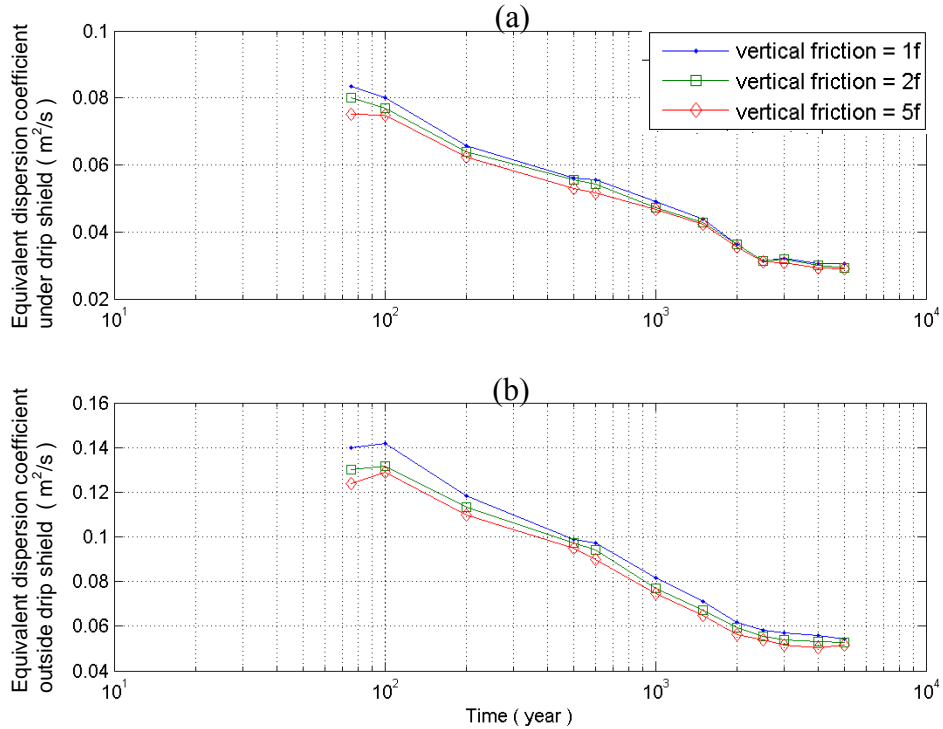


Figure 25. Sensitivity study of input friction loss coefficient, used in the air flow model, (a)inside and (b)outside the drip shield.

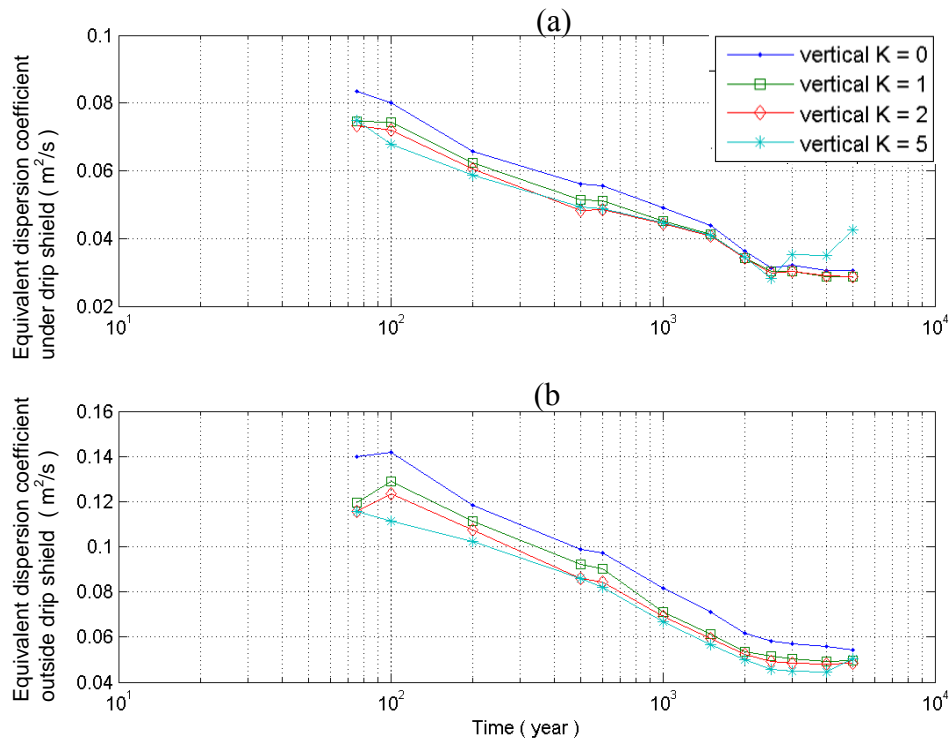


Figure 26. Sensitivity study of input kinetic shock loss factor, used in the air flow model, inside (a) and outside (b) the drip shield.

1.4 Task 1 Conclusions

- A one-directional, small air flow caused by air movement through bulkheads to neighboring drifts may cause only moderate changes in temperature. Slight asymmetry may develop between the two drift ends; the magnitude of the asymmetry is quite insignificant.
- Humidity is also only slightly affected by one-directional air migration in the drift.
- The equivalent dispersion coefficient ($0.1 \text{ m}^2/\text{s}$) for over the drip shield domain used to date in modeling is a reasonable approximation and shows a low sensitivity to the vertical friction loss coefficient and to the kinetic shock loss factor.
- Large-scale, natural, buoyancy-driven air recirculation loops will form both above and below the drip shields during post-closure. The three-dimensional velocity field is strongly coupled to the temperature and the humidity distribution requiring a fully-coupled numerical model. To date, MULTIFLUX is the only model available for solving this task.
- Large effects on lowering temperature, increasing humidity, and related increased condensation zones are seen due to natural air re-circulation in the drift. The large-scale, axial, in-drift natural air circulation is a new phenomenon that has not been seen before in publications.
- The new results obtained using the MULTIFLUX thermal-hydrologic-air flow model represents a breakthrough in coupling a porous-media model for the rockmass with a CFD model for the airspace with turbulent flow.

2 Task 2: Barometric Pressure Fluctuation Studies with a Refined Model (FY05 – FY06)

The effect of barometric pressure variation with time was re-examined during the past year with an improved numerical model, refined specifications and assumptions, and the newest conceptual waste arrangement in the emplacement drift. See details in Section 1.1 for model update information.

2.1 The Effect of Revised Model Assumptions on Moisture Influx and Condensation

The new conceptual design for Yucca Mountain includes 80 m long unheated sections at drift ends which were not included in the previous FY03 – FY04 annual report's model assumptions⁸. This modification significantly alters the moisture transport within the drift.

The effect of the unheated drift section has been studied before and found to be significant¹². The unheated section at low temperature creates a low vapor pressure point (or vapor concentration) which causes the enhanced moisture transport from the heated section toward the unheated section.

Also previously, the pressure variation was applied only at the drift level while the barometric pressure was kept constant at the surface. In FY05 and 06 modeling, this assumption was revised with the pressure variation applied both at drift level and at the ground surface simultaneously. The application of pressure only at drift level caused and enhanced moisture inflow, which resulted in more humid, and more time-variable conditions inside the heated emplacement drift.

In addition, the previous annual report⁸ did not include the effect of latent heat of condensation on the temperature field. The current analysis, using a more sophisticated MULTIFLUX model, incorporates this effect. This modification alone has caused a significant effect on the results reducing the rate of condensation in the cold sections by increasing temperatures.

Taken together, the revised model assumptions result in an enhancement factor of moisture inflow in the hot (over boiling) drift section of 4 and 0.5 times the case of average pressure ($P_{bar_{av}}$) for low ($P_{bar_{av}} - \sigma(P_{bar})$) and high ($P_{bar_{av}} + \sigma(P_{bar})$) barometric pressure, respectively. Previously⁸ the moisture flux enhancement at $P_{bar_{av}} - \sigma(P_{bar})$ was 6 to 8 times the flux at $P_{bar_{av}}$. The previous modeling results for the upper and lower relative humidity bounds on the drift surface are shown in Figure 27, and the updated modeling results are shown in Figures 28, 29, and 30 for three different segments on the drift wall circumference: the roof, the sidewall, and the floor over the invert. The 714m heated drift did not include any unheated section, while the current model is 600m with two 80m unheated sections for a total of 760m model. The lower pressure bound in Figure 27 is the base case pressure and the upper bound is $P_{bar_{av}} - \sigma(P_{bar})$; whereas the lower bound in Figures 28-30 is $P_{bar_{av}} + \sigma(P_{bar})$ and the upper bound is the same as in Figure 27.

Note that the shaded areas in Figures 27-30 represent the variation between upper and lower pressure bounds. The relative humidity will swing between the upper and lower bounding curves with a 10.66-day period time as a statistical average. The primary importance of the variations in relative humidity is that some of the accumulated salts resulting from evaporation into the drifts are hygroscopic and will deliquesce. Deliquescence can lead to dripping of concentrated salt solutions from the roof of the drifts and periodic wetting and drying cycles on a time scale measured in days.

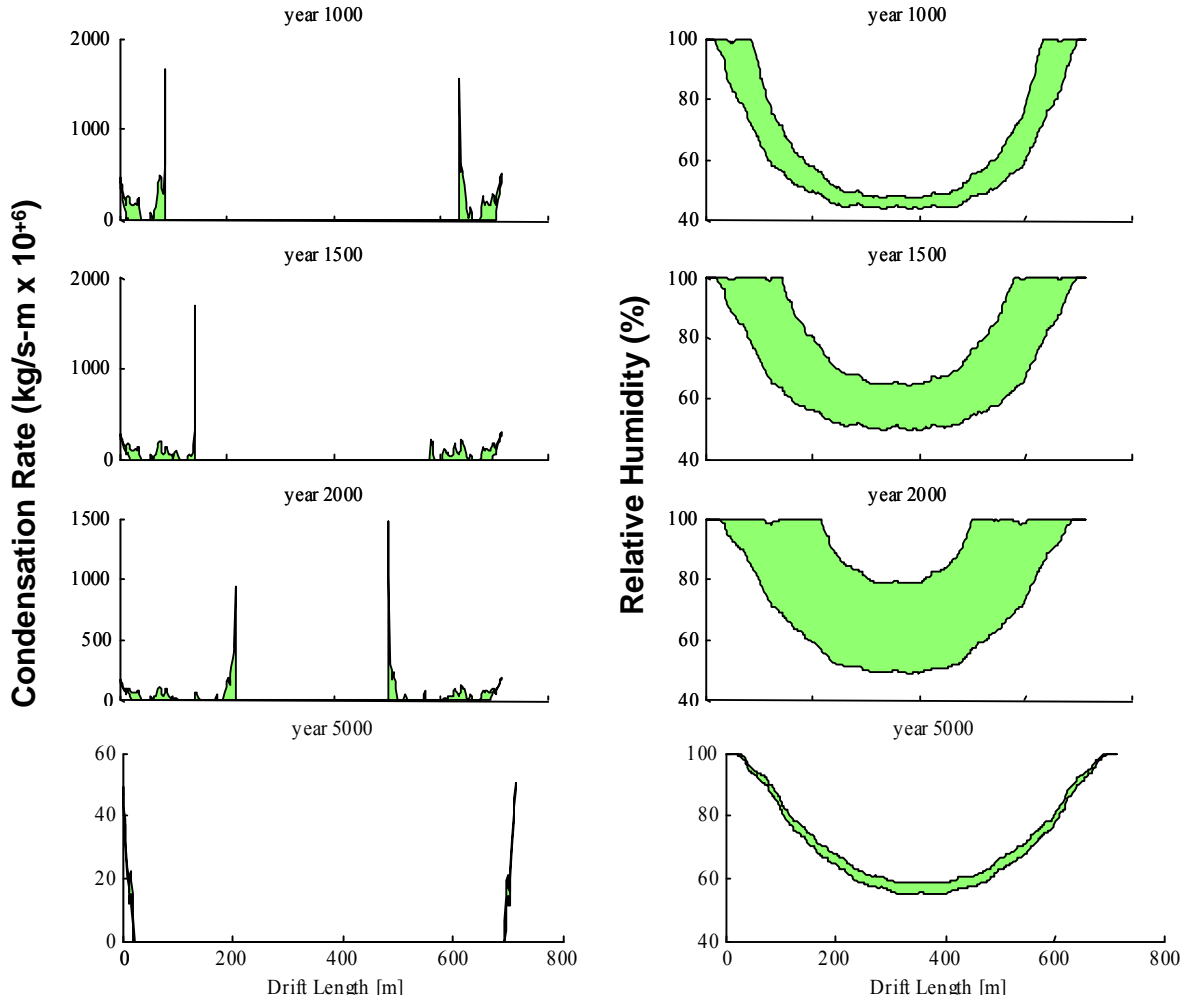


Figure 27. Barometric pressure fluctuation effects on relative humidity and condensation rate, FY03 – FY04 model results.

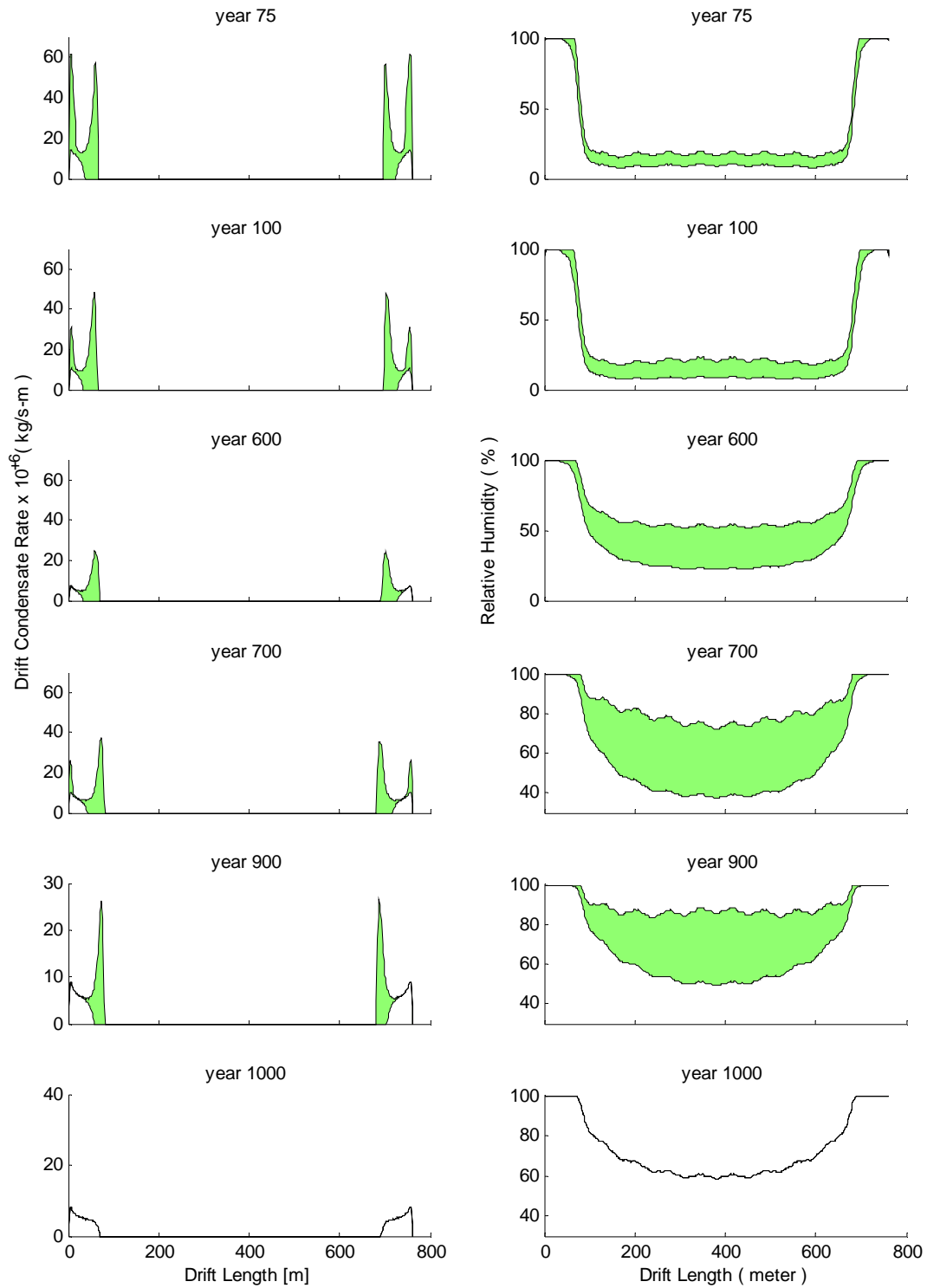


Figure 28. Barometric pressure fluctuation effects on relative humidity and condensation rate, updated FY06 model results at the roof segment of the drift wall.

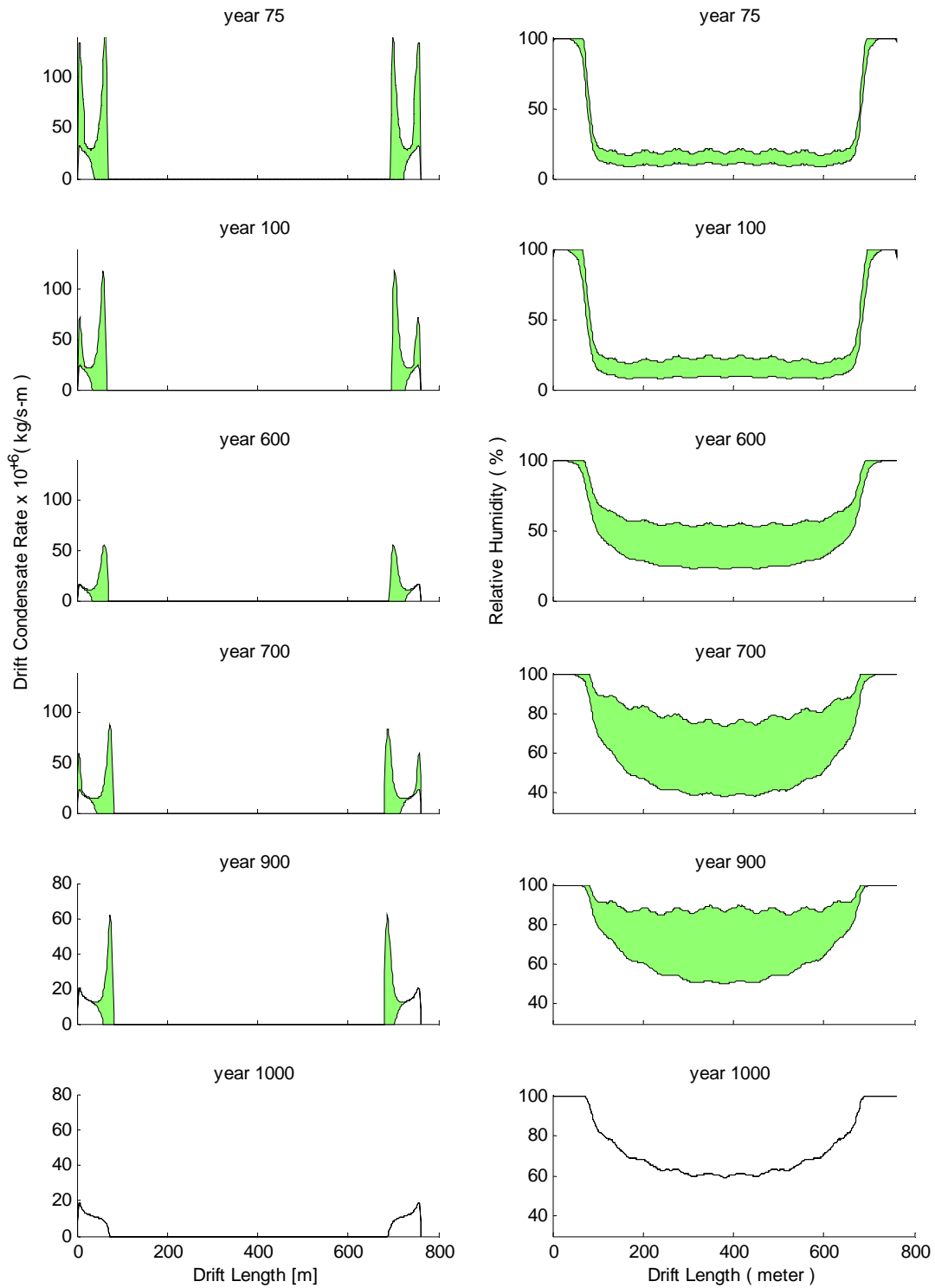


Figure 29. Barometric pressure fluctuation effects on relative humidity and condensation rate, updated FY06 model results at the sidewalls segment of the drift wall.

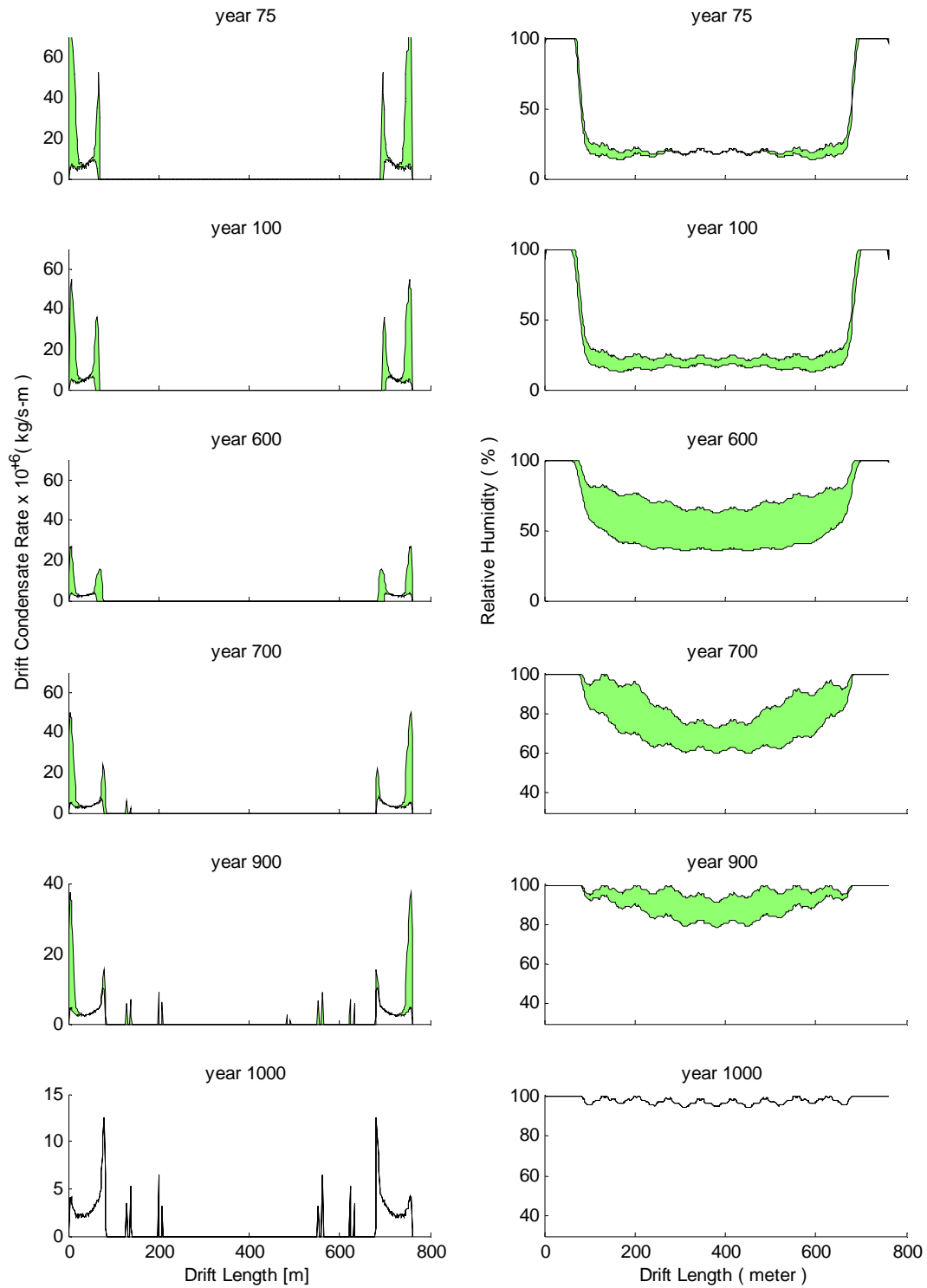


Figure 30. Barometric pressure fluctuation effects on relative humidity and condensation rate, updated FY06 model results at the floor segment of the drift wall, over the invert.

2.2 Task 2 Conclusions

- The current model uses more realistic and less conservative assumptions, resulting in significant changes in the results relative to the results of the previous study⁸.
- The overall effects of the barometric pressure variation is not as significant as it was reported⁸. Smaller range is found for the relative humidity and condensation rate fluctuations.
- One reason for the difference between the new and old results is the presence of 80-m unheated drift sections. These cold sections create a low vapor pressure area, which attracts moisture during the above boiling period.
- Another reason for the reduced enhancement of the drift moisture inflow is due to the fact that the pressure variation is simultaneously applied in the present study to both the drift level and to the ground surface. At year 1000 some condensation occurs in the heated section as a result of cold trap process caused by the variable temperature profile along the drift due to waste package heat load variations.
- Still another reason for reduced enhancement of moisture inflow is the incorporation of latent heat of condensation into the model and its effect on the temperature field.
- The pressure variation effect disappears after year 1000 when the entire emplacement drift goes below boiling. During the above boiling period of years 50-1000, the effect of pressure variation is mainly seen in the unheated sections with a few locations in the heated section showing condensation until around year 600. Variation in relative humidity is seen until around year 1000 at various parts of the hot drift section.

3 Task 3: Long-Term, Forced Ventilation Studies (FY05 – FY06)

The non-linear processes associated with the above-boiling temperature design can be mitigated by reducing temperatures. Relative humidity variation with time reduces to insignificant levels at below-boiling temperatures. Repository performance at below-boiling temperatures can be predicted with greater confidence. A series of modeling studies with open-system repository ventilation were conducted to support a conceptual solution to temperature reduction. The possibility of increasing the storage capacity, and lowering the maximum temperatures below-boiling at the same time, was also studied.

3.1 Task 3 Modeling Procedures and Results

Figure 31 shows the temperature and relative humidity variations along the drift length for 300 years of pre-closure and 5000 years of post-closure time periods for the previous baseline design without heated sections. As shown, the maximum temperatures are about the same, and close to boiling limit during (1) the 300 years pre-closure time period with cross-ventilation and (2) during the post-closure time period with no powered ventilations. These results indicate that 300 years ventilation may bring the current baseline design to below-boiling.

A doubled storage capacity with 600 years pre-closure ventilation time period was also studied as a hypothetical exercise. Figure 32 shows the temperature and relative humidity variations along the drift length for a 600 year pre-closure ventilation period and 5000 years of post-closure time periods for the current baseline design dimensions, but containing double the amount of waste assuming no waste aging. Note that temperatures are significantly below boiling for all

time periods. With waste re-processing, the necessary pre-closure ventilation cooling time period may be greatly reduced, or even eliminated.

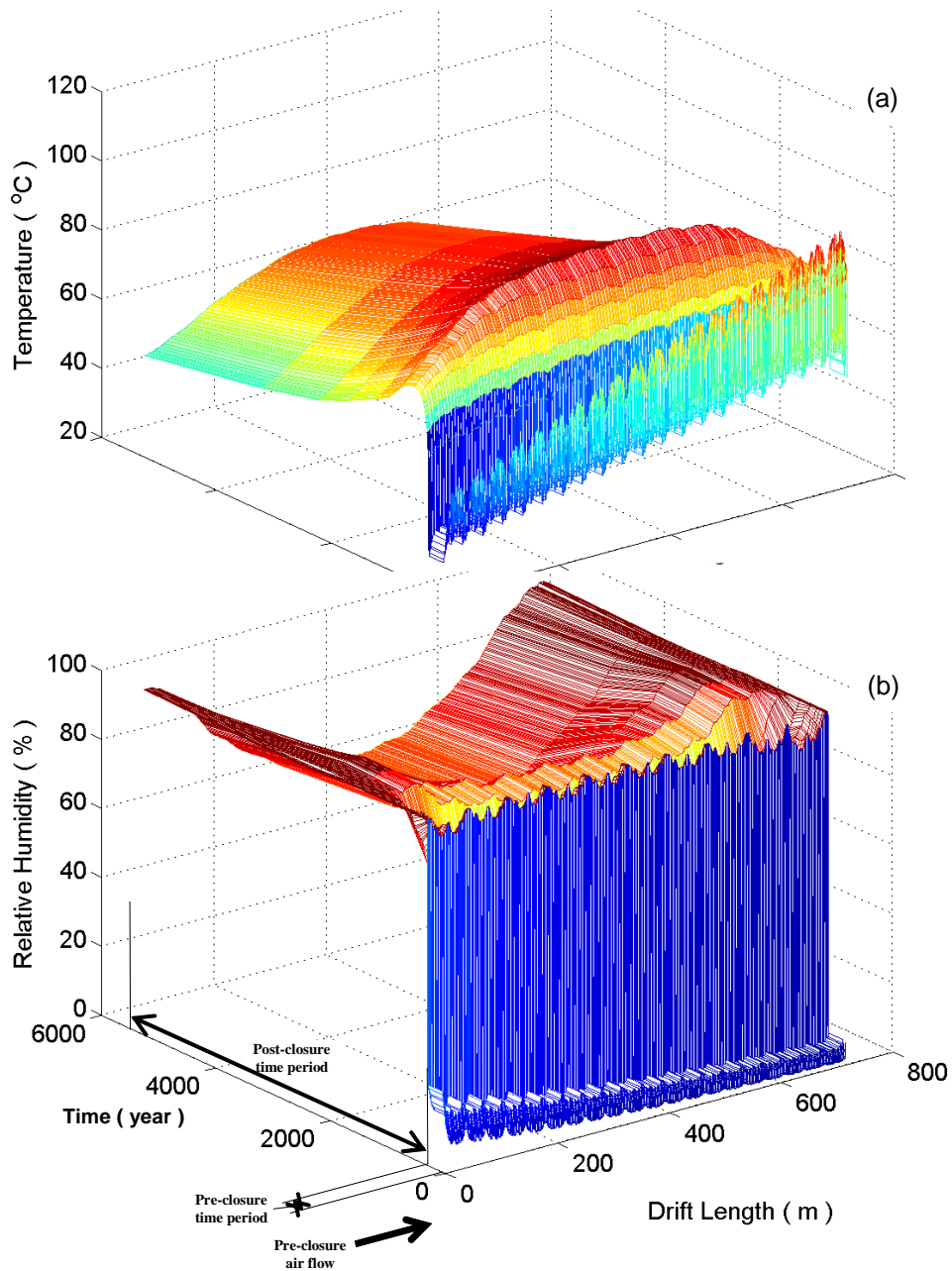


Figure 31. Long-term, forced ventilation studies (300 years), baseline results.

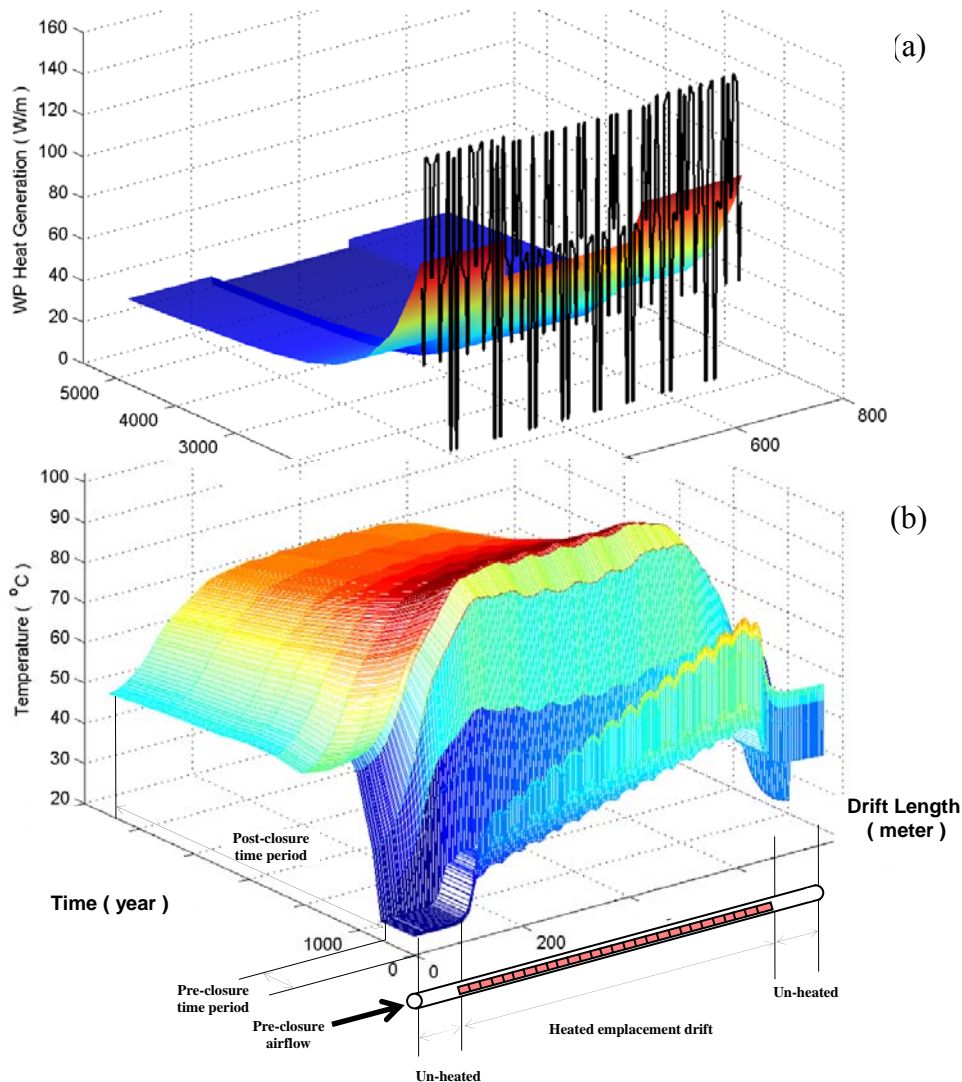


Figure 32. Variable, optimized post-closure heat load per unit length for individual WPs at year 600 (solid line), and line-averaged load equivalent (smooth surface) (a); temperature variation of a double-capacity, low-temperature, conceptual repository (b); and relative humidity (c); all with 600 years pre-closure ventilation, assuming no waste re-processing.

3.2 Task 3 Conclusions

- A below-boiling temperature design with doubled storage capacity may be achieved with 600 years pre-closure ventilation, assuming no waste re-processing. With waste re-processing, the necessary pre-closure ventilation cooling time period may be greatly reduced, or even eliminated.
- Change to a below boiling repository would reduce the potential for localized corrosion during the thermal period since (a) Alloy-22 is more resistant to localized corrosion at lower temperatures; (b) at below boiling temperatures the accumulation of salts will be

less; and (c) at below boiling temperatures, the barometric pressure changes will no longer lead to cycles of variations in relative humidity and condensation.

4 Task 4: In-rock vapor flow studies (FY05 – FY06)

Examination of modeled liquid water and vapor flow directions in the rockmass around the emplacement drift provides evidence for total evaporation in this region of rock, and reinforces the salt accumulation hypothesis and deliquescence briefly mentioned in Section 2.

4.1 Task 4 Description of Modeling and Results

The revised rockmass model described in Sections 1 and 2 was used for the rockmass surrounding the emplacement drift. It was a post-closure study of 5000 years time period, preceding with 50-year pre-closure cooling by forced ventilation. No barometric pressure variation or air infiltration in the drift was assumed during post-closure.

Results for the above-boiling temperature, baseline design from the new model are shown in Figures 33a and b for temperature and relative humidity distributions on the drift wall with time and along the length. Slight variations in the results with the drift length are caused by the heat dissipation variations between individual WPs.

Figure 34a shows spatial and temporal variations of condensation. The vapor inflow into the drift air space is depicted in Figure 34b in the form of the water attraction ratio, a non-dimensional ratio between the spatial and temporal vapor flux into the drift and the percolation water flux calculated over the springline width, D , of the drift. The W in the W/D water attraction ratio may be pictured as an imaginary width over which the natural ambient water percolation flux is collected, and transported into the drift by evaporation or seepage. The $W/D=1$ isoline is marked in Figure 34b. In the domain where $W/D>1$, the drift is effectively a water attractor. This domain approximately coincides with the spatial and temporal domain where the temperature is above-boiling.

Evaporation in the rockmass around the drift naturally means that dissolved ions from the source water will precipitate and accumulate as solids. Total evaporation of the percolation water flow as well as the pore water initially present in the rock matrix represents a source of solid species that must precipitate according to mass conservation. It is possible to estimate the accumulation over the drift crown numerically using the percolation flux towards the drift footprint for the time period over which the evaporation is complete, evidenced by dead-end percolation flow patterns. Figure 34c is an upper estimate of chloride ion (Cl^-) accumulation, associated with the total evaporation of water over the drift width, D , as a function of the axial position along drift length and time. The chloride accumulation at this point is a hypothesis based on the assumption that the concentration of chloride in pore water is 117 mg/L at YM^{13} , and that the total amount of chloride is deposited in the rock wall during complete evaporation. The numerical model results are used only within the boundaries of total evaporation with no dissolution due to lack of percolating liquid water leaving a control volume of the rockmass. Further trends are indicated in Figure 34c as possible continuations with and without salt discharge. Two processes are in competition in the rockmass at the front of evaporation: (1) salt thickening (by liquid water

evaporation) and (2) discharge (by water flow transport). The rate of deposition or dissolution is a complex phenomenon that can be modeled with TOUGHREACT¹⁴. However, during total evaporation and no liquid water discharge from a rockmass volume, a simple estimation of salt accumulation is possible without using a kinetic model.

Figure 35a through f are liquid water and vapor flow patterns from the NUFT model-element in the fractured and porous rockmass surrounding the emplacement drift in its middle section at three different time instants. Until year 1500, at which time the drift is already slightly below-boiling, all percolating water disappears and turns into vapor form. The liquid water flow above the drift will dead-end in the rockmass, and become a vapor source, as shown in the diverging vapor flow fields in Figure 35b and d. A very small diversion of the percolation water flow at the drift crown is seen at year 2000 in Figure 35e, indicating the onset of potential solute discharge and the effect of drift shadow. Vapor flow is still active all around the perimeter including the drift crown and the floor, as depicted in Figure 35f, showing that vapor accumulation above the drift and vapor discharge into the floor of the drift may coexist for some time.

4.2 Task 4 Conclusions

- One consequence of the high temperature operation mode is that the vapor flow into the drift must give rise to salt accumulation in the rock wall, especially in the crown of the drift, during the above-boiling time period, when evaporation of the water percolation is complete. This conclusion is supported by the analysis of total evaporation, and water mass balance in the rock above and around the emplacement drift, evidenced by vapor and water flow fields calculated by NUFT, shown in Figures 35a to d.
- Another consequence of the high temperature operation mode is that the variable vapor flow, as a modulation due to barometric pressure variation, creates fluctuating relative humidity in the emplacement drift. The drift wall at certain locations may vary between dry and wet conditions periodically over time.
- Salt accumulations in conditions conducive to flow separation of anions, combined with relative humidity cycling may create a potentially more aggressive corrosion environment than currently being considered for the above-boiling design.

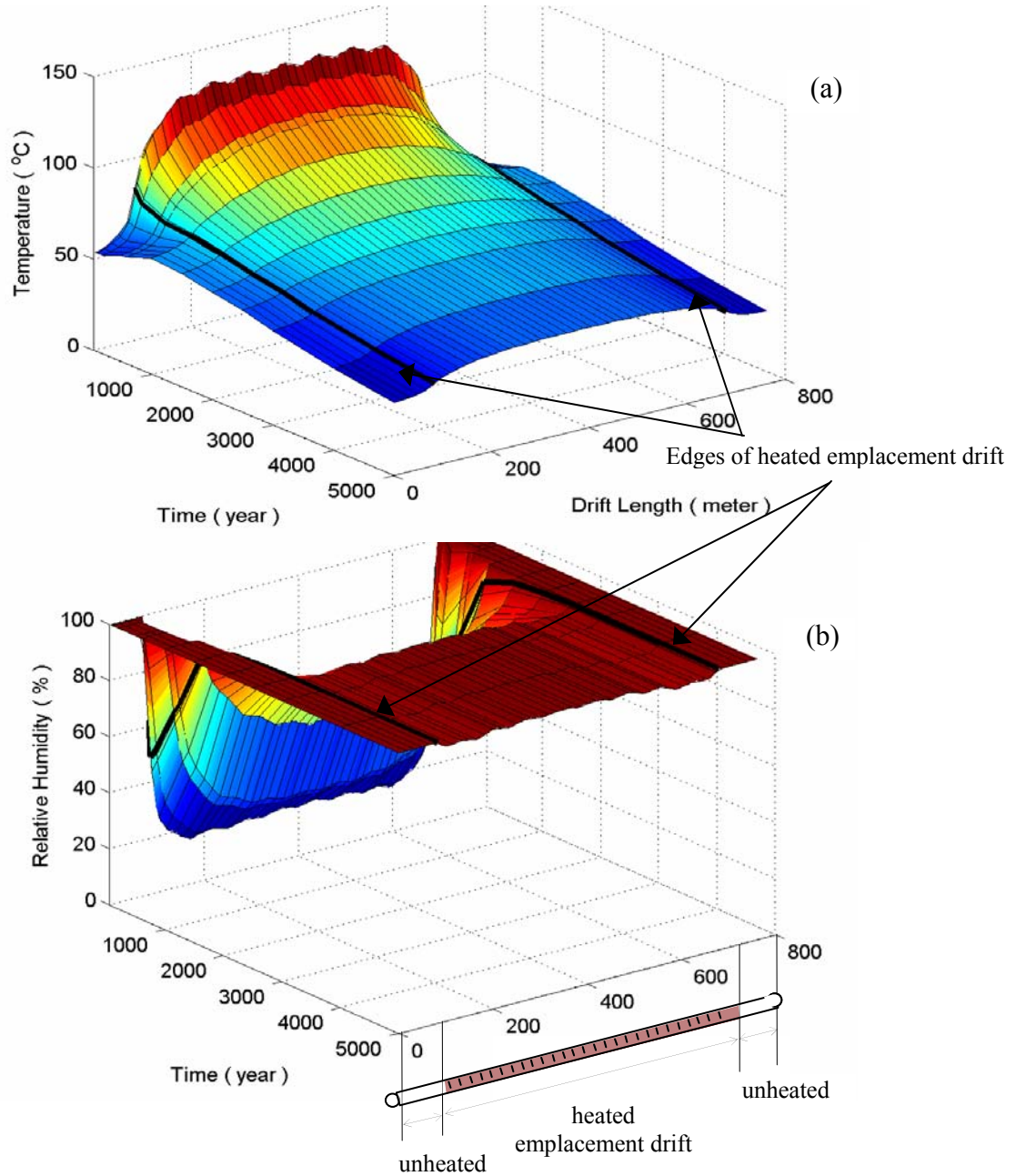


Figure 33. In-rock (via drift) vapor flow studies, drift wall temperature (a) and wall relative humidity (b) distribution in time and space.

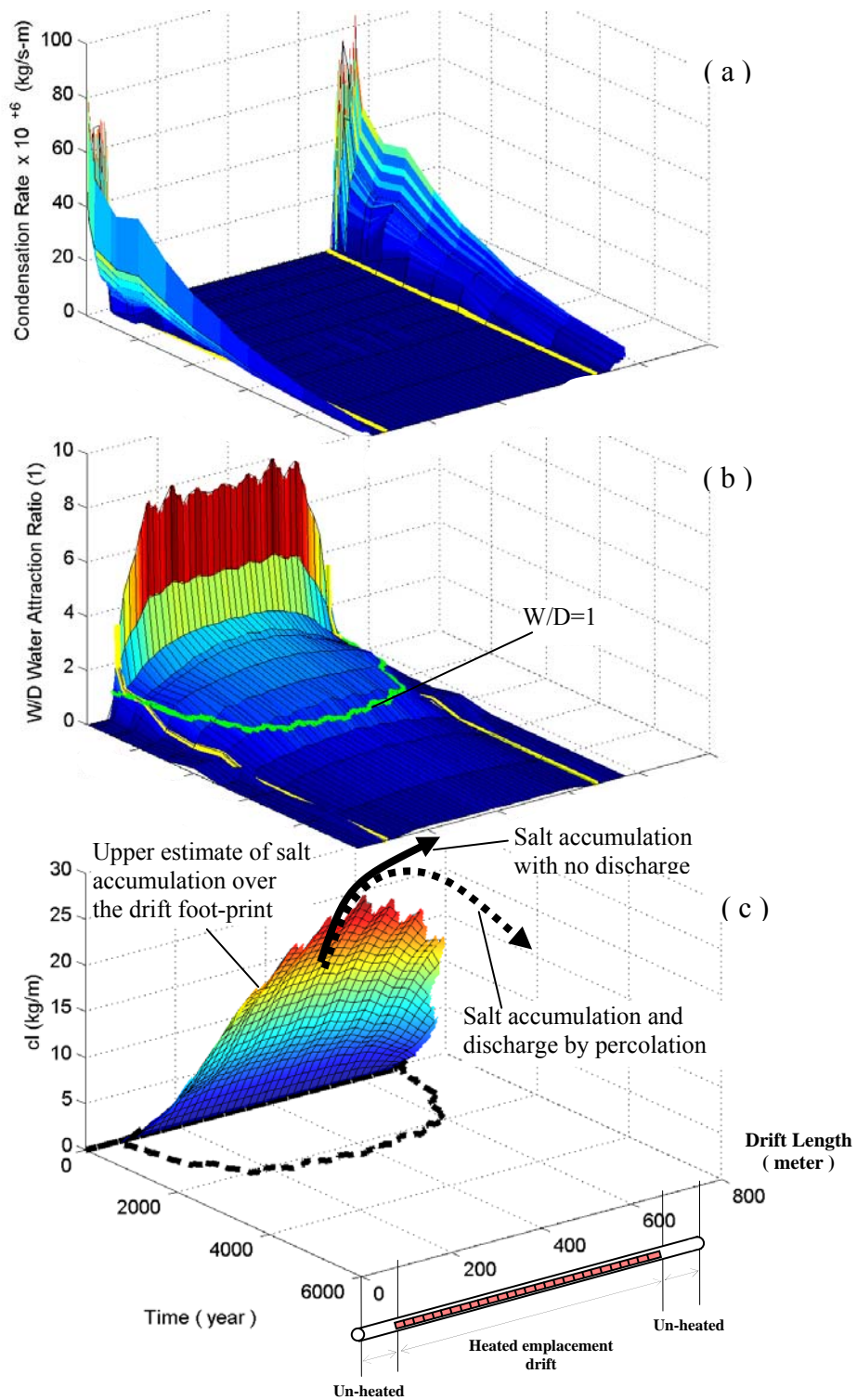


Figure 34. Water condensation rate at the emplacement drift wall (a); W/D water attraction ratio (b); chloride accumulation over the drift width D (c); as a hypothesis from the model results.

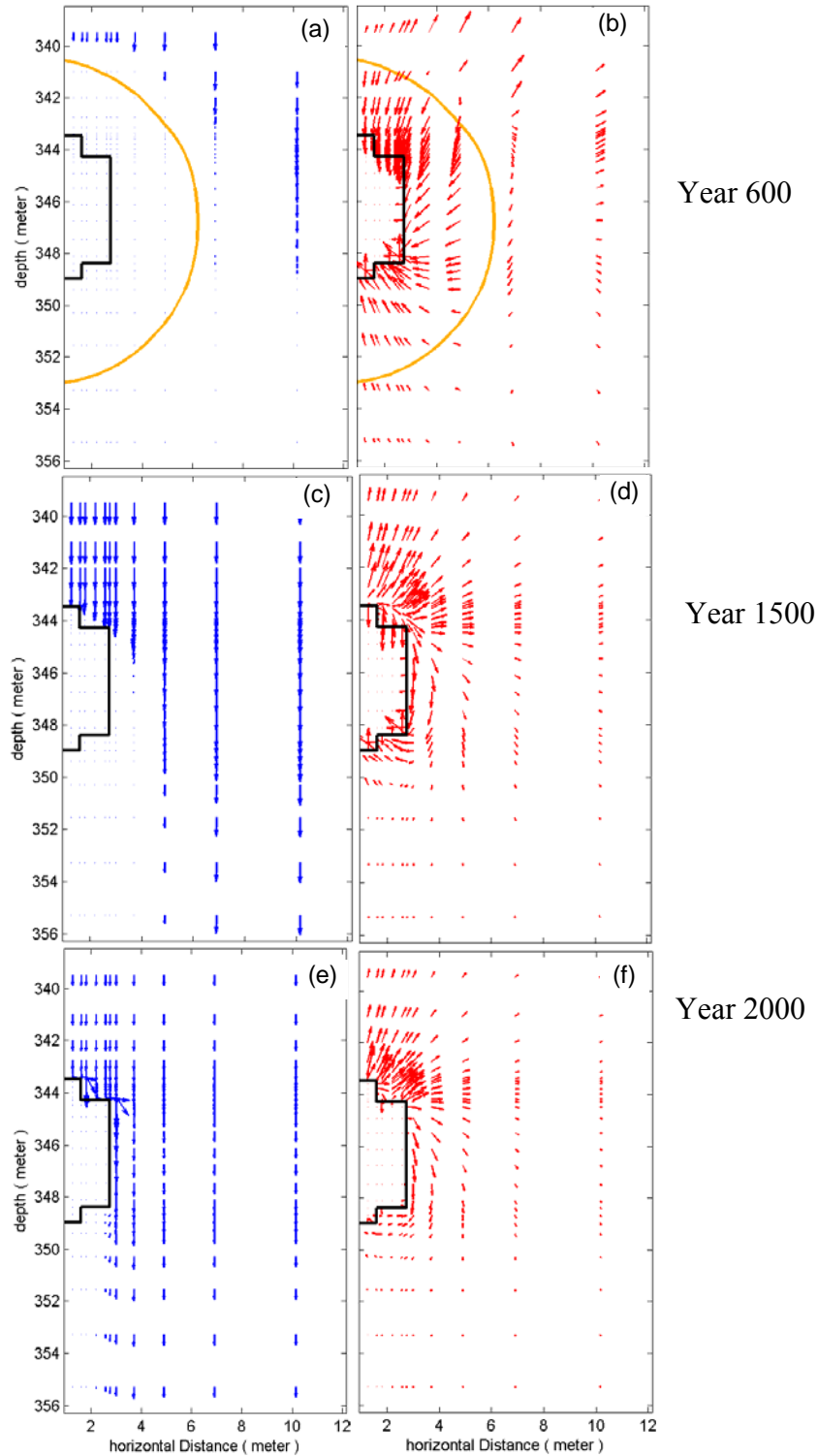


Figure 35. Water pore velocity in the rock mass surrounding the emplacement drift in liquid phase (left column, a, c, e) and gas phase (right column, b, d, f) at year 600 (a, b); year 1500 (c, d); and year 2000 (e, f); solid line indicates 96 °C contour, the boiling temperature at Yucca Mountain.

5 Major Ventilation Modeling Conclusions and Recommendations

The main conclusion of the studies is that the convective heat and moisture transports have a major influence upon the temperature and humidity conditions and resulting condensation in and around the drifts both during the pre- as well as post-closure time periods. Consequently, any thermal-hydrologic model that is designed to predict the likely operating environment at Yucca Mountain with a reasonable degree of certainty must have the capabilities of incorporating the heat and mass transport represented by laminar or turbulent air flow during both pre- and post-closure operation.

This finding is diagonally opposite to what has been used as a working hypothesis in the Multi-Scale Thermal Hydrologic (MSTH) modeling concept, applied to the YMP for analysis and design. According to the MSTH model results, the axial flow of heat and moisture is insignificant and has no impact on the thermal-hydrologic storage environment. The effects of this contention may be far-reaching.

The presence of axial transport is expected to affect the operating environment during the first few thousand years. The higher the temperature regime, the larger impact is expected and so is the uncertainty created by the absence of axial transport in DOE's process models. On the other hand, at below-boiling operating temperature, the axial transport is indeed insignificant, reducing with other factors, modeling complexity and uncertainty.

Long-term ventilation is seen as a viable technology for reducing operating temperature even if the storage capacity is increased at the same time, relative to the waste load density in the baseline design.

MULTIFLUX has grown into a fully capable numerical model that has proven to solve the coupled in-drift and in-rock transport processes with full drift simulations with turbulent flows during both pre- and post-closure operations.

Such a modeling capability will be needed for explaining performance confirmation measurements at Yucca Mountain from the onset of operations. Nye County has a vested interest in monitoring the relevant processes at play at Yucca Mountain that includes air discharges into the accessible environment. Through the coupled in-rock and in-air transport processes, the exhaust air parameters from the emplacement drifts and the air shafts have an important and intricate confirmatory value to understanding the entire thermal-hydrologic-air process evolution at Yucca Mountain.

References

1. Bahrami, D. and Danko, G., (2006). “Thermal-Hydrologic Model of an Alternative Waste Package Design for Yucca Mountain Repository.”, *Journal of Nuclear Technology*, Vol. 154, pp. 247-264.
2. Danko, G., Bahrami, D., (2006). “The Effect of Pre-Closure Ventilation on the Environmental Conditions at Yucca Mountain.”, *Proceedings, Int. High-Level Radioactive Waste Management Conference*. Las Vegas, 2006.
3. Danko, G., Bahrami, D., (2006). “Barometric Pressure Variation Effects on Emplacement Drift Environmental Conditions at Yucca Mountain.”, *Proceedings, Int. High-Level Radioactive Waste Management Conference*. Las Vegas, 2006.
4. Bahrami, D., Danko, G., and Walton, J., (2006). “Water, Vapor, and Salt Dynamics in a Hot Repository.”, *Material Research Society*, 2006 Fall meeting.
5. Danko, G., Walton, J., and Bahrami, D., (approved). “Increased Storage Capacity at Yucca Mountain Favors Thermal Management for a Cold Repository.”, (approved for publication in the *Journal of Nuclear Technology*, 2007).
6. G. Danko, (2006) “Functional or Operator Representation of Numerical Heat and Mass Transport Models.”, *ASME J. of Heat Transfer*, Vol. 128, pp. 162-175.
7. Walton, J, G. Danko, and D. Bahrami, (2006). “Effect of cyclic, sporadic, or episodic processes on evolution of environments in a repository in Yucca Mountain.”, *Invited Presentation at the Nuclear Waste Technical Review Board Corrosion Workshop*, Las Vegas, NV, September, 2006.
8. NWRPO (Nuclear Waste Repository Project Office). (2005). “Coupled Hydrothermal-Ventilation Studies for Yucca Mountain Annual Report For April 2004-March 2005.”, *Technical Report No. NWRPO-2005-02*. Pahrump, Nevada: Nuclear Waste Repository Project Office. September 2005. 176 p.
9. Danko G., J. Birkholzer and D. Bahrami, (2007), “Thermal-Hydrological Near-Field Model Studies and Impact of Natural Convection of Seepage.”, 2nd Quarterly report for Office of Science and Technology and International.
10. Birkholzer, J., N. Halecky, S.W. Webb, P.F. Peterson, G.S. Bodvarsson, 2006. “The Impact of Natural Convection on Near-Field TH Processes at Yucca Mountain.” *Proceedings, 11th International High-Level Nuclear Waste Conference*, April, Las Vegas, NV.
11. DOE (U.S. Department of Energy). 2004b. “Multiscale Thermohydrologic Model.” Prepared by Bechtel SAIC Company, LLC. ANL-EBS-MD-000049 REV 01. Yucca Mountain Project. Las Vegas, Nevada.
12. Danko, G., Bahrami, D., Birkholzer, J.T., (2006). “The Effect of Unheated Sections on Moisture Transport in the Emplacement Drift.”, *Proceedings, Int. High-Level Radioactive Waste Management Conference*. Las Vegas, 2006.
13. DOE, 2000. Yucca Mountain Project Technical Database [TDR-NBS-MD-000001, 2000].

14. Xu, T. and Pruess, K., 2001. *Modeling Multiphase Non-Isothermal Fluid Flow and Reactive Geochemical Transport in Variably Saturated Fractured Rocks: 1. Methodology*. American Journal of Science, Vol. 301, January, pp. 16-33.